arXiv:1101.3375v1 [astro-ph.GA] 18 Jan 2011

Multicolor Photometry Study of the Galaxy Cluster A2589: Dynamics, Luminosity Function and Star Formation History

Shun-Fang Liu[1,2,3], Qi-Rong Yuan[4], Yan-Bin Yang[1,3], Jun Ma[1,3], Zhao-Ji Jiang[1,3], Jiang-Hua Wu[1,3],
Zhen-Yu Wu[1,3], Jian-Sheng Chen[1,3], Xu Zhou[1,3]

`liusf@bac.pku.edu.cn; yuanqirong@njnu.edu.cn; zhouxu@bao.ac.cn`

ABSTRACT

Smooth X-ray morphology and non-detection of radio source at center indicate that A2589 is a typical case of well-relaxed regular galaxy cluster. In this paper we present a multicolor photometry for A2589 ($z = 0.0414$) with 15 intermediate bands in the Beijing-Arizona-Taiwan-Connecticut (BATC) system which covers an optical wavelength range from 3000 Å to 10000 Å. The spectral energy distributions (SEDs) for more than 5000 sources are achieved down to $V \sim 20$ mag in about 1 deg^2 field. A2589 has been also covered by the Sloan Digital Sky Survey (SDSS) in photometric mode only. A cross-identification of the BATC-detected galaxies with the SDSS photometric catalog achieves 1199 galaxies brighter than $i = 19.5$ mag, among which 68 member galaxies with known spectroscopic redshifts are found. After combining the SDSS five-band photometric data and the BATC SEDs, the technique of photometric redshift is applied to these galaxies for selecting faint member galaxies. The color-magnitude relation is taken as a further restriction of early-type cluster galaxies. As a result, 106 galaxies are newly selected as member galaxies. Spatial distribution of member galaxies shows a north-south elongation which agrees with the X-ray brightness profile and the orientation of central cD galaxy, NGC 7647. No substructures are detected on the basis of positions and radial velocities of cluster galaxies, indicating that A2589 is a well-relaxed system. The luminosity function of A2589 exhibits a peak at $M_R \sim -20$ mag and a dip at $M_R \sim -19$ mag. The low-density outer regions are the preferred habitat of faint galaxies. With the evolutionary population synthesis model, PEGASE, the environmental effect on the star formation properties for 68 spectroscopically confirmed member galaxies is studied. The outlier faint galaxies tend to have longer time scales of star formation, shorter mean stellar ages, and lower metallicities of interstellar medium, which can be interpreted in the context of hierarchical cosmological scenario.

Subject headings: galaxies: clusters: individual (A2589) – galaxies: distances and redshifts — galaxies: kinematics and dynamics — galaxies: evolution — methods: data analysis

---

[1] National Astronomical Observatories, Chinese Academy of Sciences, Beijing 100012, China

[2] Graduate University, Chinese Academy of Sciences, Beijing, 100039, China

[3] Key Laboratory of Optical Astronomy, National Astronomical Observatories, Chinese Academy of Sciences

[4] Department of Physics, Nanjing Normal University, Nanjing , China

1. Introduction

As the largest gravitationally bound systems in the universe, galaxy clusters play a central role in cosmological studies, such as the baryon content of the universe, formation of large-scale structure, and the density parameters in cosmological models (Bahcall 1996). For instance, the distribution of cluster velocity dispersions and mass-to-light ratios might provide limits on the amplitude of primordial density fluctuations in hierarchical clustering scenarios (Evrard 1989; Frenk et al. 1990). In the cold dark matter models, galaxy clusters are complex multicomponent systems where galaxies, hot gas, and dark matter evolve in a tightly coupled way (Frenk et al. 1996), and they are driven by accreting these components along filaments (Bekki 2001; Roettiger et al. 1996; Navarro & White 1994; Cen & Ostriker 1994). Therefore, cluster of galaxies has been regarded as a powerful laboratory for studying the evolution of the galaxies in a dense environment where the physical properties of galaxies might have been influenced by many different mechanisms, including strong galaxy-galaxy interaction (Mihos 2004), harassment (Moore, Lake & Katz 1998), ram pressure stripping (Quilis et al. 2000), and strangulation (Bower & Balogh 2004, also known as starvation, or suffocation).

According to the hierarchical clustering scenario, galaxy clusters continue to be assembled, and relaxation is not yet complete in most clusters. It is widely appreciated that a regular cluster with no detectable substructure both in spatial distribution and in velocity space is at the most evolved stage. However, significant substructures have been revealed in a large number of rich galaxy clusters with the X-ray imaging and optical spectroscopic surveys (Rhee & Latour 1991; Forman & Jones 1982; Beers et al. 1991; Sarazin et al. 1992; Henry & Briel 1993; Burns et al. 1994). Numerical simulation of the evolution of galaxy clusters indicates that at least 50% of apparently relaxed clusters contain significant substructures (Salvador-Sole et al. 1993). Very few clusters with single central dominant cD galaxy are found to be spherically symmetric in distributions of galaxies and hot gas. Even for the Coma cluster that was once regarded as an exemplar of regular and well-relaxed cluster, the projected distributions of galaxies and the X-ray-emitting gas also show convincing evidence of significant substructures on large and small scales (Colless & Dunn 1996; White et al. 1993; Neumann et al. 2003). Recently, a deep spectroscopic survey for the faint galaxies in the central region of Coma cluster has confirmed previously identified substructures, and found three new substructures (Adami et al. 2009). Despite shortage of well-relaxed cD galaxy clusters, for a better understanding of the evolution of galaxies, the clusters at the final evolution stage are worthwhile to be extensively investigated with multiwavelength data. In addition, the well-relaxed clusters of galaxies are important laboratories for studying the dark matter in clusters. Because hot gas in the core regions of such clusters is undisturbed by interactions with the central radio source, it is relatively straightforward to resolve the spatial distribution of the gravitation matter which is dominated by the dark matter (Buote & Lewis 2004).

The regular cluster of galaxies A2589 (z=0.0414), located at $23^h24^m00^s.5$, +16°49′29″.0 (J2000.0), with Abell richness R=0 (Abell 1958) and BM type I (Bautz & Morgan 1970), is particularly well suited for such analysis. It appears remarkably relaxed and does not show any obvious signs of ongoing mergers. According to the ROSAT images, A2589 is a cluster with a smooth X-ray morphology (Buote & Tsai 1996), and the ROSAT PSPC observation reveals a cool gas temperature ($kT \sim 3$ keV) and a high X-ray luminosity ($L_{0.5-2.0\mathrm{keV}} \sim 8.5 \times 10^{43}$ ergs s^{-1}) for the central region of A2589, defined by a radius of 0.5

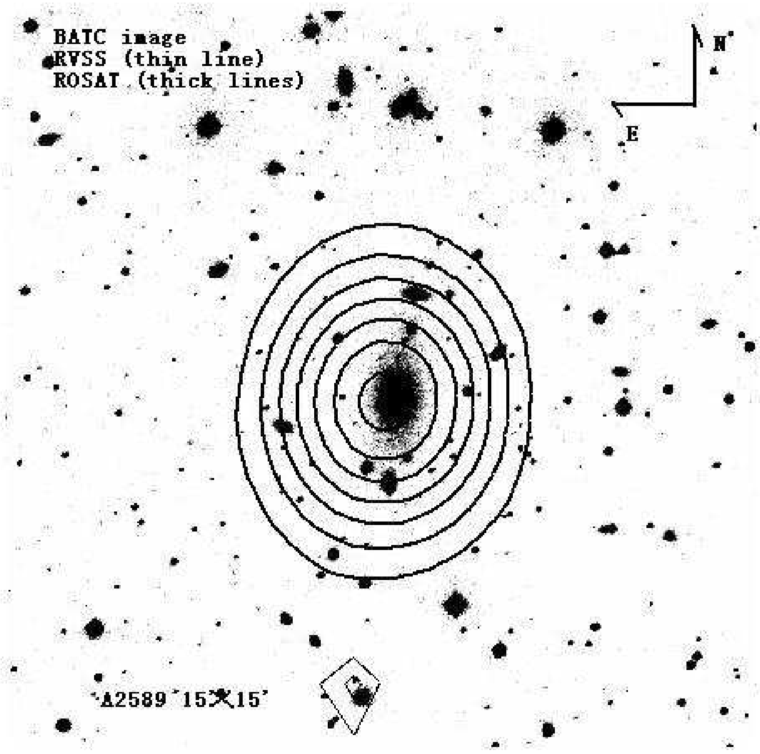

Fig. 1.— The smoothed contours of the ROSAT PSPC image in soft X-ray band (0.1-2.4keV) (*thick line*) and of the NVSS map at 1.4 GHz (*thin line*), superimposed on optical image of $15' \times 15'$in the BATC h band. The sizes of gaussian smoothing windows are adopted as $30''$and $2'$for the radio and X-ray contours, respectively.

Mpc (David et al. 1996). The $Chandra$ image with higher spatial resolution shows no substantial morphological disturbance and no cooling flow in the core of A2589 (Buote & Lewis 2004). Mccarthy et al. (2004) supposed an entropy injection mechanism to explain the relaxed status of the “non-cooling flow” cluster A2589. Additionally, no bright radio source is detected at the cluster center by the NRAO VLA Sky Survey (NVSS) (Bauer et al. 2000).

Previous optical studies of the galaxies in A2589 also show no evidence supporting the presence of subclusters (Beers et al. 1991). It is still a tough task to spectroscopically cover all the dwarf galaxies with low surface brightness (Kambas et al. 2000). As mentioned above, A2589 is not a rich cluster. Abell (1958) appraised its richness as R=0, which means less than 50 member galaxies within the magnitude range m_3 to $m_3 + 2$ (where m_3 is the magnitude of the third brightest galaxy). The multicolor optical photometry therefore becomes an alternative way for picking up faint member galaxies in a cluster. According their spectral energy distributions (SEDs), the redshifts of galaxies can be estimated by the technique of photometric redshift. The Beijing-Arizona-Taiwan-Connecticut (BATC) photometric survey is designed for such purpose, and allows us to study the properties of member galaxies in nearby ($z < 0.1$) clusters (Yuan et al. 2001, 2003; Yang et al. 2004; Zhang et al. 2010).

The relaxed and structureless appearance of A2589 can be well shown by Figure 1, which presents the smoothed contours of the ROSAT All-Sky Survey (RASS) image in soft X-ray band (0.1-2.4keV) and of the NVSS map at 1.4 GHz, superimposed on optical image of $15' \times 15'$in the BATC h band. In this paper we will present a multicolor photometric study of the relaxed cluster A2589, using 15 intermediate filters of the BATC system which covers an optical wavelength region from 3000 to 10000 Å. The paper is organized as follows. In Section 2, we describe the BATC observation and data reduction. The SED selection of faint cluster galaxies is given in Section 3. In Section 4, we will show the main results about spatial distribution, dynamics, luminosity function, and star formation properties of cluster galaxies. Finally, summary and perspective will be given in Section 5. Throughout this paper we adopt the ΛCDM cosmology model with H_0=70 km s^{-1} Mpc^{-1}, Ω_m=0.3 and Ω_Λ=0.7.

2. Observations and Data Reduction

2.1. BATC Observation

The observations of A2589 were carried out with the BATC filter system which includes 15 intermediate-band filters, namely, $a-k$, and $m-p$, covering the whole optical wavelength range. These intermediate filters are specifically designed to avoid most of the known bright night-sky emission lines (Yan et al. 2000), and they are mounted on the 60/90 cm f/3 Schmidt Telescope at the Xinglong station, National Astronomical Observatories of China (NAOC). Before October 2006, the BATC system was equipped with an old 2048 $\times$ 2048 Ford CCD camera. The field of view was about 1 square degree, and the spatial scale was $1.7''$per pixel. For pursuing a better spatial resolution and a higher sensitivity in blue bands, a new E2V 4096 $\times$ 4096 CCD is now put into service. This CCD has a quantum efficiency of 92.2% at 4000 Å and a spatial scale of $1.35''$per pixel. The field of view is extended to $92' \times 92'$. The pixel sizes for the old and new CCD cameras are 15 and 12 μm, respectively, corresponding to a pixel size ratio of 5:4. The details of the telescope, camera, and data-acquisition system can be found elsewhere (Zhou et al. 2001; Yan et al. 2000). For distinguishing explicitly between the SDSS and BATC filter names, in this paper, we refer to the SDSS filters and magnitudes as *u'*, *g'*, *r'*, *i'*, *z'*, with their central wavelengths of 3560, 4680, 6180, 7500 and 8870Å. The transmissions of the BATC and SDSS filters can be seen in Yuan et al. (2003).

From September 2002 to November 2005, only 12 BATC filters, from *d* to *p*, were taken to target A2589 with the old CCD, discontinuously. Since 2006, the exposures in *a, b, c* bands have been completed with new CCD camera. In total, we have made 169 images with more than 54 hr of exposure, which were selected to be combined. The details of A2589 observation are given in Table 1.

2.2. Data Reduction

The bias substraction and dome flat-field correction were done on the CCD images by using *Pipeline I* (Fan et al. 1996; Zhou et al. 2001) , the automatic data reduction code for the BATC survey. The cosmic-

Table 1: Parameters of the BATC Filters and the Observational Statistics of A2589

No.	Filter name	λ_c^a (Å)	FWHM (Å)	Exposure (s)	Seeing^b (arcsec)	Completeness magnitude	Indival Exposure (s)	frames
01	a	3369.4	277.6	32400	3.99	20.5	1200	27
02	b	3921.3	265.5	19200	3.70	20.5	1200	16
03	c	4205.6	288.5	13800	3.76	20.5	900	14
							600	2
04	d	4528.9	370.6	12000	5.45	21.0	1200	20
05	e	4884.7	372.4	13200	5.01	21.0	1200	11
06	f	5225.1	333.8	9600	5.08	21.0	1200	8
07	g	5793.8	284.5	7200	4.07	20.0	1200	6
08	h	6093.6	310.4	6000	4.24	20.0	1200	5
09	i	6093.6	310.4	5101	4.41	19.5	1200	4
							301	1
10	j	7032.3	163.0	6000	4.38	19.5	1200	5
11	k	7539.5	197.2	9000	4.29	19.0	1200	7
							300	2
12	m	8012.7	286.6	12000	4.21	19.0	1200	10
13	n	8509.5	168.2	11414	4.35	19.0	1200	9
							614	1
14	o	9172.9	248.4	18000	3.97	18.5	1200	15
15	p	9740.7	272.0	19200	3.85	18.5	1200	16

^{a} Central wavelengths of the filters; ^{b} This column lists the seeings of the combined images.

ray and bad pixel effects were corrected by comparing the images. Before combination, the images were recentered, and the position calibration was performed by using the Guide Star Catalog (GSC) (Jenkner et al. 1990).

For detecting sources and measuring the source fluxes within a given aperture in the combined BATC images, *Pipeline II*, a photometry package developed on the basis of DAOPHOT (Stetson 1987) kernel (Zhou et al. 2003), is taken to perform aperture photometry. The objects with signal-to-noise ratio greater than the threshold 3.5 σ in i, j, and k bands will be detected. Considering the pixel size ratio of 5:4 between the old and the new CCDs, we take an aperture radius of 4 pixels (i.e. r=1.″7×4=6.″8) for the images in 12 bands (d to p), and a radius of 5 pixels (i.e., r=1″.35×5=6.″8) for the images in *a,b,c* bands. Flux calibration in the BATC system is performed by using four Oke-Gunn standard stars (HD 19445, HD 84937, BD+262606 and BD+17 4708) (Gunn & Stryker 1983), whose fluxes have been slightly corrected by further BATC observations during photometric nights (Zhou et al. 2001). To check the results of flux calibration via standard stars, we then perform the model calibration on the basis of the stellar SED library (Zhou et al. 1999). The flux measurements derived by these two calibration methods are in accordance with each other for most filters. As a result, the SEDs of 3465 sources are achieved down to $i = 19.5$ within our field of view.

For assessing the measurement errors in specified magnitude, we compared the errors using different subgroups of magnitudes with an interval of 0.5 mag. We find that magnitude error in each filter becomes larger at fainter depth. Errors in the $a-n$ bands are found to be less than 0.02 mag for stars with $i < 16.5$, and more than 0.05 mag for stars with $i > 19.0$.

3. Selection of faint member galaxies in A2589

3.1. Combing the BATC and SDSS SEDs

Owing to low spatial resolution of the BATC images, it is difficult to make star-galaxy separation via the surface brightness profiles of detected sources. Alternatively, the color-color diagram is a powerful tool for morphological classification. Fortunately, A2589 has been covered by the SDSS photometric survey, and the star-galaxy classification of all sources down to $r' = 22.0$ has been performed via their light profiles. After a cross-identification of these 3465 sources detected by the BATC photometry with the SDSS photometric catalog, we obtain a list of 1199 galaxies brighter than $i = 19.5$ within the BATC field of $58' \times 58'$. For checking the completeness of the BATC detection of galaxies, we compare the SDSS galaxies down to a same brightness depth (i.e., r' <19.5) in the same region. Within central region with a radius of 0.5 degree, there are 555 SDSS-detected galaxies among which 537 galaxies are detected by the BATC, corresponding to a completeness of BATC detection of 96.8%. Spacial scale at cluster redshift $z = 0.0414$ is 0.818 kpc/arcsec, the typical seeing of combined images in the BATC bands is about 4.2 arcsec, corresponding to 3.4 kpc, which is smaller than the size of a typical spiral galaxy. With the photometric catalog of SDSS galaxies, a cross-identification of the 1199 galaxies with i<19.5 is performed for estimating the percentage of object blending due to the seeing effect. A searching circle with a radius of 4.3 arcsec centered at BATC galaxies is adopted, and 27 galaxies are found to have more than one counterpart within the searching circle. The overall blending percentage is about 2.25%. We divide the BATC galaxies into 4 subsamples with the i-band magnitude interval of 1.0 mag, ranging from 15.5 to 19.5, the blending percentage are 2.63%, 4.21%, 2.08%, 2.03%, respectively.

Furthermore, we take use of the NASA/IPAC Extragalactic Database (NED) to extract available observational information of the bright galaxies on the list. There are 81 galaxies having known spectroscopic redshifts. Note that A2589 has not been covered by the SDSS spectroscopic survey, the available spectroscopic redshifts of galaxies are contributed by relevant literature (Bothun & Schombert 1988; Capelato et al. 1991; Wegner et al. 1999; Smith et al. 2004; Haynes et al. 1997). Majority of spectroscopic redshifts were obtained by Smith et al. (2004), and their selection criteria for spectroscopy are: $R < 17.0$ and $\Delta(B-R) > -0.2$. For estimating completeness of spectroscopic sample, we apply the same criteria to the SDSS photometric data. By using the equations in Lupton (2005), the SDSS magnitudes can be transformed into B and R magnitudes. As a result, 111 SDSS galaxies are found to satisfy the criteria. Figure 2 shows the histograms of these 111 SDSS galaxies and 81 galaxies with known spectroscopic redshifts. The overall spectroscopic completeness down to $R = 16.5$ should be about $58/78 \sim 74\%$. Since only 30% of the faint galaxies with $16.5 < R < 17.0$ are spectroscopically covered, the overall completeness down to $R = 17.0$ decreases to $68/108 \sim 63\%$.

For a given galaxy detected by the SDSS imaging observation, two models were used to fit the observed

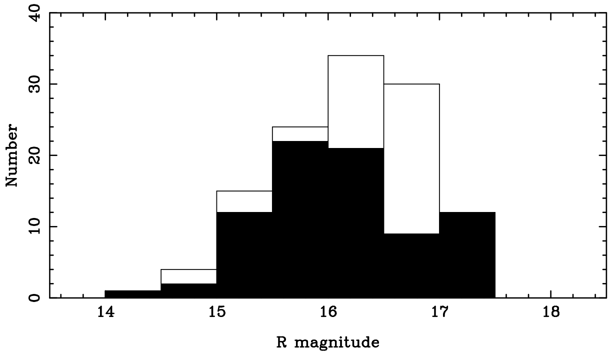

Fig. 2.— The histograms of the 111 SDSS galaxies selected by the criteria: $R < 17.0$ and $\Delta(B-R) > -0.2$, superposed with the histrogram of 81 galaxies with known spectroscopic redshifts (hatched region).

surface brightness profile: (1) the de Vaucouleurs model, and (2) the exponential model. For measuring unbiased colors of galaxies, we use the dereddened SDSS model magnitudes which are measured by their flux through equivalent apertures in all SDSS bands. The model (exponential or de Vaucouleurs) of higher likelihood in the r filter is chosen, and then applied (i.e., allowing only the amplitude to vary) in the other SDSS bands after convolving with the appropriate PSF in each band. Because the resulting model magnitudes are calculated using the best-fit parameters in the r' band, the light is measured consistently through the same aperture in all SDSS bands.

Figure 3(a) shows the relative SDSS and BATC SEDs of the central cD galaxy in A2589, NGC 7647. It is clear that there is a systematic offset between two SEDs which is called zero point. A method of interpolation is applied to derive the zero point. Due to a larger magnitude error in the u' band, the magnitude offsets for other four SDSS filters are calculated by the interpolation algorithm on the basis of the BATC magnitudes in neighboring bands, and then take the average of the second and third largest offsets as the SED zero point. Figure 3(b) gives the combined SED of NGC 7647 after zero point correction. The zero point distribution for all the galaxies is presented in Figure 4. It can be seen that the peak of the zero point is -0.2 mag, indicating that the aperture of $r = 6.''8$ is large enough to hold the majority of galaxies and to make different seeing effect negligible. For the most extended central cD galaxy, NGC 7647, our aperture just covers its core region, which leads to a large zero point of nearly 2.0 mag. After zero point correction, the combined 20-band SEDs for 2101 galaxies detected by BATC and SDSS photometry are achieved.

3.2. Sample of spectroscopically-confirmed member galaxies

Figure 5 shows the distribution of spectroscopic redshifts for 81 galaxies, with the bin size 0.001. The bulk of the spectroscopic redshifts is concentrated between 0.03 and 0.06, corresponding to A2589. In order to eliminate the background galaxies, we convert the spectroscopic redshifts (z_{sp}) for the galaxies with $0.03 < z_{sp} < 0.06$ into rest-frame velocities (V) by $V = c(z_{sp} - \bar{z}_c)/(1 + \bar{z}_c)$, where c is the light speed, $\bar{z}_c$ is the cluster redshift with respect to the cosmic background radiation. We take the NED-given cluster

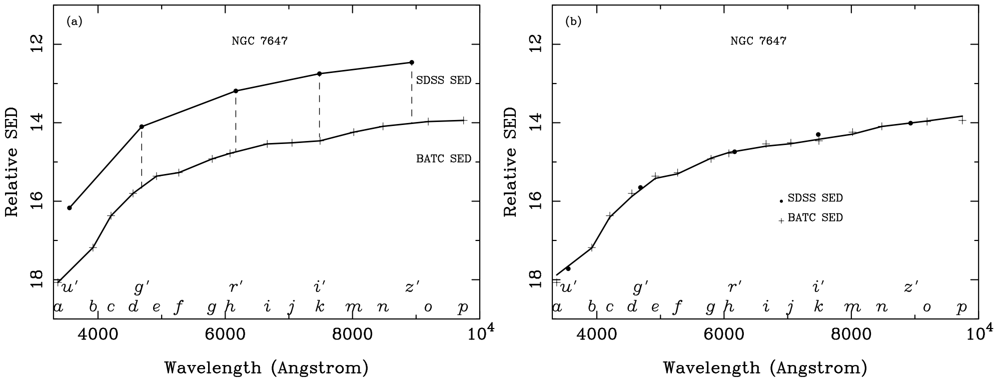

Fig. 3.— Relative SEDs in the BATC and SDSS systems for the central cD galaxy, NGC 7647, in A2589. (a) before zero point correction (SED connections are denoted by solid lines, and zero points in g', r', i', z' bands are denoted by dashed lines); (b): after the zero-point correction (The solid line represents the best-fit model SED.)

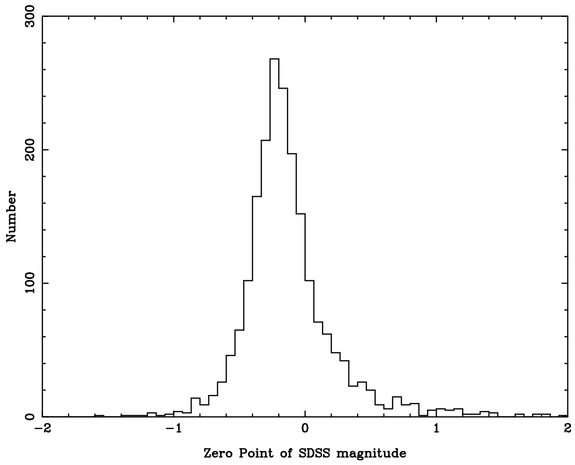

Fig. 4.— Distribution of the zero points for the galaxies brighter than $i = 19.5$ detected by both multicolor surveys.

redshift of $\bar{z_c} = 0.0414$ for A2589 (Struble & Rood 1999). A Gaussian fit is then applied to the distribution of rest-frame velocities, and a dispersion of σ=751 km s^{-1} is derived. With the prevalent selection criterium of 3σ clipping, 68 galaxies with $-2215 < V < 2293$ km s^{-1}, corresponding to the z_{sp} range from 0.034 to 0.048, are selected as member galaxies, to which we refer as "sample I". Table 2 lists the SDSS-given celestial coordinate in degrees and the spectroscopic redshift in literature for these 68 member galaxies in sample I, in order by right ascension. The embedded panel of Figure 5 shows the histogram of rest-frame velocities for sample I with Gaussian fit.

With only 26 member galaxies in cluster A2589, Capelato et al. (1991) derived a Gaussian velocity distribution with $\mu_{\rm cz} = 12437 \pm 91 \ {\rm km\,s^{-1}}$and $\sigma = 415^{+119}_{-58} \ {\rm km\,s^{-1}}$. Based on 30 member galaxies, Beers et al. (1991) characterized the distribution of measured galaxy velocities by using the ROSTAT software. Two resistant and robust estimators (namely, the biweight location C$_{\rm BI}$ and scale S$_{\rm BI}$), analogous to

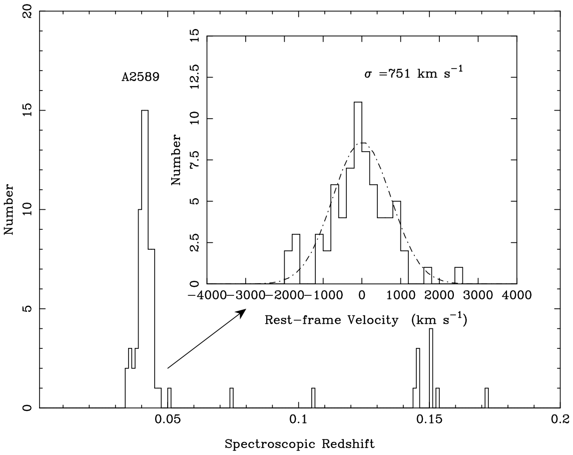

Fig. 5.— Distribution of spectroscopic redshifts for 81 galaxies detected by both multicolor surveys. The embedded panel shows the histogram of rest-frame velocities for 68 member galaxies.

the velocity mean and standard deviation, are defined to characterize the velocity distribution (Beers et al. 1990). Beers et al. (1991) found C$_{\rm BI}$=12475$^{+199}_{-139}$ km s^{-1}and S$_{\rm BI}$=624$^{+457}_{-274}$ km s^{-1}. For 68 spectroscopically confirmed member galaxies, we use the ROSTAT software to calculate the biweight location and scale, and achieve C$_{\rm BI}$=12122 $\pm$ 90 km s^{-1}and S$_{\rm BI}$=737 $\pm$ 85 km s^{-1}. Comparatively, the biweight location in our statistics is smaller, and the biweight scale is larger with smaller uncertainties. In addition, the ROSTAT statistics for the velocity distribution shows that the number of big gaps is 0, which means the A2589 might be a virialized system.

3.3. Photometric Redshift Technique

It is well known that the technique of photometric redshift can be used to estimated the redshifts of galaxies on the basis of the SED information given by multicolor photometric surveys. With the development of large and deep field survey, this technique has been widely applied (Lanzetta et al. 1996; Arnouts et al. 1999; Furusawa et al. 2000). Based on the standard SED-fitting code called HYPERZ (Bolzonella et al. 2000), the procedures for estimating the photometric redshifts have been developed especially for the BATC multicolor photometric system (Yuan et al. 2001; Xia et al. 2002). For a given object, the photometric redshift, z$_{ph}$, corresponds to the best fit (in the χ^2-sense) between its photometric SED and the template SED. The SED templates for the normal galaxies are generated by convolving the galaxy spectra in template library with the transmission curves of the BATC and SDSS filters. In our SED fitting, we take the templates of normal galaxies in the GISSEL98 (Galaxy Isochore Synthesis Spectral Evolution Library) (Bruzual & Charlot 1993). The dust extinction with a reddening law of Milky Way (Allen 1976) is adopted, and the A$_V$ is flexible in a range from 0.0 to 0.5, in steps of 0.05. As a test, we firstly let the photometric redshift vary in a wide range from 0.0 to 1.0, with a step of 0.01. Only five galaxies are found to have $z_{ph} > 0.5$. Then we search the z_{ph} values for 1199 galaxies brighter than $i = 19.5$ in a range from 0.0 to 0.5, with a smaller step of 0.005.

Table 2: Catalog of 68 Spectroscopically Confirmed Member Galaxies in A2589

No.	R.A.	Decl.	$z_{\rm sp}$	Ref.	No.	R.A.	Decl	$z_{\rm sp}$	Ref.
1	350.62835693	16.51060104	0.037286	(4)	35	350.99468994	16.79987144	0.040638	(1)
2	350.64688110	16.70728493	0.040188	(4)	36	350.99569702	16.87491226	0.044764	(3)
3	350.65444946	16.48854637	0.037256	(4)	37	350.99636841	16.81119919	0.042606	(3)
4	350.65954590	17.08135414	0.039137	(4)	38	350.99871826	16.87028122	0.040695	(4)
5	350.72991943	17.12408638	0.039671	(4)	39	351.00134277	16.82041550	0.034737	(1)
6	350.74523926	16.82660675	0.041102	(4)	40	351.00775146	16.81094170	0.035578	(4)
7	350.76705933	16.88853836	0.039070	(4)	41	351.01373291	16.77923775	0.041235	(1)
8	350.79455566	16.91345406	0.041068	(3)	42	351.02078247	16.87013626	0.041295	(3)
9	350.79602051	16.43208885	0.044357	(4)	43	351.02178955	16.66199303	0.040985	(4)
10	350.83938599	16.94395256	0.043143	(4)	44	351.02416992	16.79190254	0.041689	(4)
11	350.85235596	17.02542877	0.039898	(4)	45	351.02755737	16.54348183	0.040064	(4)
12	350.87240601	16.86256027	0.043313	(4)	46	351.03936768	17.11158180	0.039734	(4)
13	350.87268066	16.38849258	0.043523	(4)	47	351.03942871	16.66924858	0.044077	(4)
14	350.88140869	17.15295792	0.043557	(4)	48	351.04479980	16.53371620	0.039234	(4)
15	350.88894653	16.66280174	0.039150	(2)	49	351.05325317	17.10195732	0.044361	(4)
16	350.90270996	16.43026352	0.039961	(4)	50	351.06170654	16.73438454	0.037609	(4)
17	350.90341187	16.56361008	0.044487	(4)	51	351.06555176	16.78513336	0.041382	(2)
18	350.92968750	16.81964874	0.038477	(4)	52	351.07147217	16.92798424	0.041732	(4)
19	350.94128418	16.64007378	0.040208	(4)	53	351.08148193	16.73162270	0.044461	(3)
20	350.94842529	16.85229111	0.041812	(3)	54	351.08395386	16.55175018	0.043470	(4)
21	350.94931030	16.75221825	0.035171	(3)	55	351.09353638	17.04872704	0.041415	(4)
22	350.95083618	16.76874352	0.047183	(4)	56	351.09497070	17.19940758	0.042426	(4)
23	350.95123291	16.70607948	0.042019	(4)	57	351.09564209	16.80035019	0.042386	(4)
24	350.96112061	16.69865799	0.039157	(4)	58	351.13067627	16.86814690	0.035628	(5)
25	350.96188354	16.89692116	0.040441	(4)	59	351.13531494	17.10596466	0.040848	(4)
26	350.96264648	16.52305412	0.042426	(4)	60	351.14495850	16.68141174	0.040405	(3)
27	350.96414185	16.64476776	0.034701	(3)	61	351.17916870	17.13553810	0.041292	(4)
28	350.96905518	16.87223816	0.042670	(2)	62	351.19665527	16.94142342	0.043236	(4)
29	350.97305298	16.88004684	0.044984	(4)	63	351.24346924	16.53924561	0.042186	(4)
30	350.97683716	16.68067169	0.045195	(3)	64	351.30581665	16.40709877	0.039030	(4)
31	350.98266602	16.91675758	0.041212	(4)	65	351.30831909	16.82109833	0.043984	(4)
32	350.98645020	16.75003433	0.038326	(4)	66	351.33325195	17.02133942	0.041022	(4)
33	350.98931885	16.77722740	0.041118	(3)	67	351.33901978	16.68581009	0.041722	(4)
34	350.99304199	16.75839233	0.041949	(4)	68	351.39672852	16.54359245	0.041722	(4)

References: (1) Bothun & Schombert (1988); (2) Capelato et al. (1991); (3) Wegner et al. (1999); (4) Smith et al. (2004); (5) Haynes et al. (1997)

During performing the HYPERZ, we develop an iterative method to discard the bad magnitudes in the observed SED. For a given galaxy, the first running of the HYPERZ gives the best-fit template SED, and the observed magnitude at a specified filter with the maximum deviation from the best-fit SED is selected. If its maximum deviation excesses 5 times of magnitude error, we will discard this magnitude in the observed SED, and search for the best SED fitting again. In the worst case, three magnitudes in an observed SED are allowed to be discarded in order to obtain a more accurate photometric redshift.

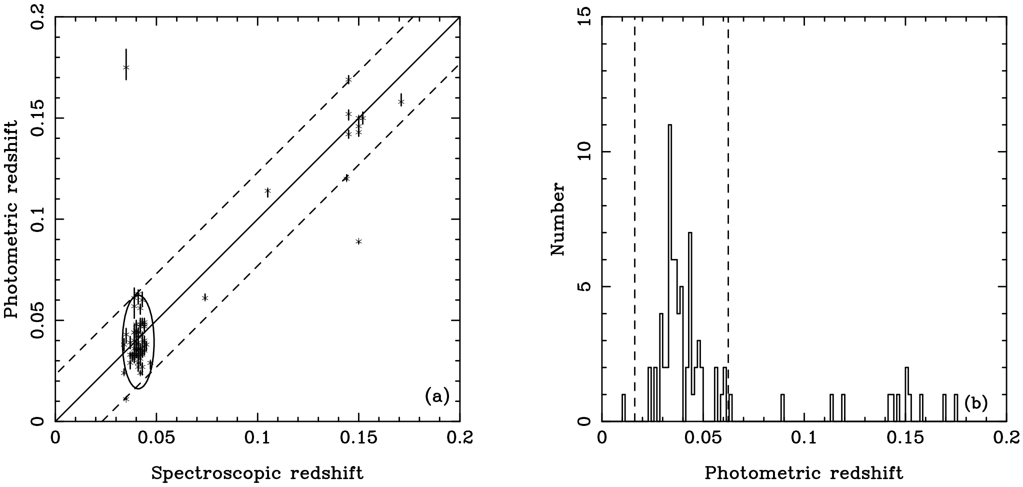

Fig. 6.— Left: Comparison between photometric redshift (z_{ph}) and spectroscopic redshift (z_{sp}) for 81 galaxies with known spectroscopic redshifts in the region of A2589. Right: The distribution of photometric redshifts of 81 known spectroscopic redshift galaxies. The dash lines are the 3σ range of the photometric redshift.

As a result, we obtain the photometric redshifts for 1199 galaxies brighter than $i = 19.5$, including the 81 galaxies with known z_{sp} values. Figure 6(a) shows the redshift comparison for these 81 galaxies. It is obvious that our z_{ph} estimate is basically consistent with the z_{sp} values. For the 68 member galaxies, the mean photometric redshift is 0.0393, and the standard deviation is 0.0077. The solid line denotes to z_{ph}=z_{sp}, and the dash lines indicate $\pm 3\sigma$ deviations (i.e., $3 \times 0.0077 = 0.023$) in the z_{ph} estimate, and the error bar of z_{ph} corresponds to 68$\%$ confidence level in our z_{ph} determination. Considering the selection algorithm of 3σ clipping in the z_{ph} space, 66 (about 97%) of 68 member galaxies have their z_{ph} values between 0.016 and 0.062 (i.e., $\bar{z}_{ph} \pm 3\sigma$), only two spectroscopically confirmed member galaxies are missed out. This z_{ph} range (shown in Figure 6(b) with the dashed lines) is taken as a selection criterium to select the member candidates from the remaining 1118 ($= 1199 - 81$) galaxies without z_{sp} values. Figure 7(a) shows the average $|z_{ph} - z_{sp}|$ as a function of the BATC *i*-band magnitude. The four magnitude bins are defined as i <15.5, 15.5< i <16.0, 16.0< i <16.5, and i >16.5. The standard errors of $|z_{ph} - z_{sp}|$ are 0.0066, 0.0041, 0.0027, 0.0135, respectively. **A similar statistics of z_{ph} uncertainties for 1199 galaxies is given in Figure 7(b), indicating that the z_{ph} uncertainty given by the SED-fitting code HYPERZ also depends upon the magnitude. The four magnitutde bins are defined as 15.5 $<$ i <16.5, 16.5< i <17.5, 17.5< i <18.5, 18.5< i <19.5, and their standard errors are 0.0011, 0.0018, 0.0037, 0.0104, respectively. For the faint galaxies with greater magnitude errors, the degree of SED fitting tends to be worse, which results in larger uncertainties.**

After applying the z_{ph}-technique to the combined SEDs of 1118 galaxies, 110 faint galaxies (including 73 early-type galaxies and 37 late-types) are found as member galaxies candidates of A2589. Figure 8 shows the z_{ph} histograms for the galaxies in different detection depths. Panel (a) gives the z_{ph} distribution for the 171 bright galaxies with $i < 17.5$, and panel (b) is for the 1199 galaxies with $i < 19.5$. The dash

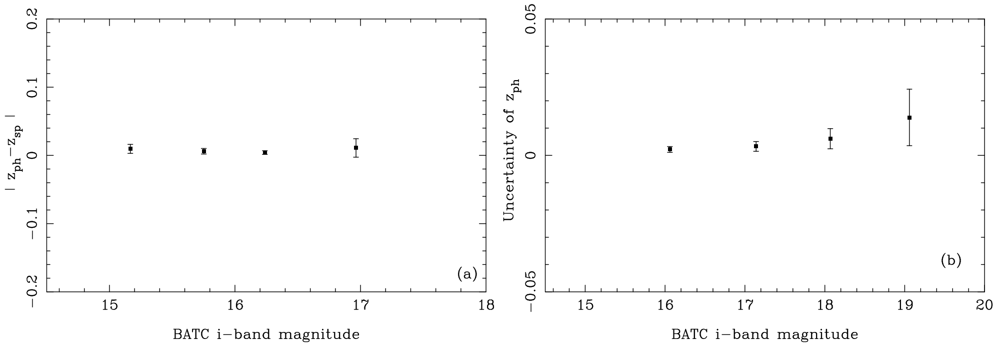

Fig. 7.— Left: Plot of the average deviations , $|z_{ph} - z_{sp}|$, and standard errors (denoted by error bars) as a function of BATC *i*-band magnitude. The four magnitude bins are defined as i <15.5, 15.5< i <16.0, 16.0< i <16.5, i >16.5. The standard errors of $|z_{ph} - z_{sp}|$ are 0.0066, 0.0041, 0.0027, 0.0135, respectively. **Right: Plot of the uncertainty of 1199 photometric redshit as a function of BATC *i*-band magnitude. The four magnitutde bins are defined as 15.5 $<$ i <16.5, 16.5< i <17.5, 17.5< i <18.5, 18.5< i <19.5, and their standard errors are 0.0011, 0.0018, 0.0037,0.0104, respectively.**

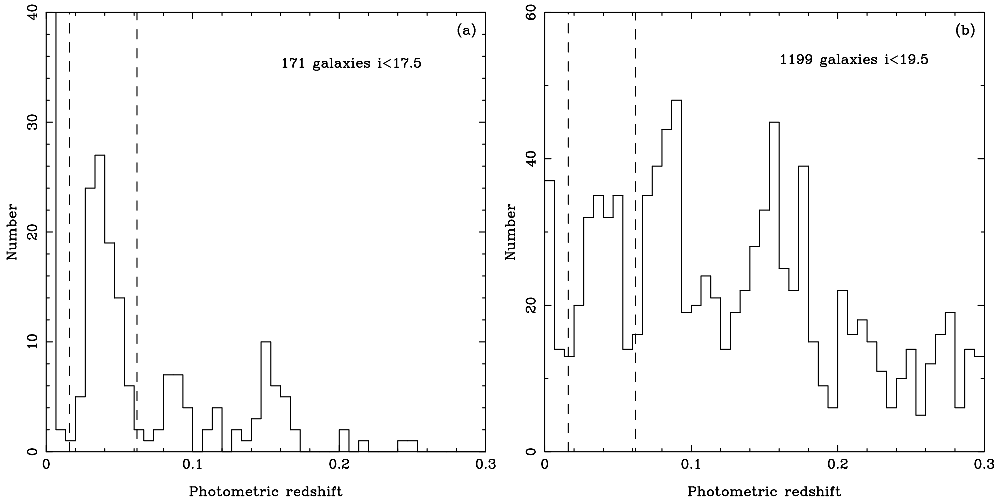

Fig. 8.— Distributions of estimated photometric redshifts for (a) 171 galaxies brighter than $i = 17.5$; (b) 1199 galaxies brighter than $i = 19.5$.

lines are denoted as the photometric redshift range of cluster member candidates. At the detection depth of $i = 17.5$, corresponding to the limit of the SDSS spectroscopy, the peak at $z_{ph} = 0.04$ (contributed by cluster A2589) is very prominent. As the magnitude limit goes to the faint end, the peak of A2589 is still remarkable though a large number of background galaxies are detected, which demonstrates the reliability of our method of combining the BATC and SDSS photometric data and the SED-fitting procedure.

3.4. The Color-Magnitude Correlation

A correlation between color and absolute magnitude for early-type galaxies, the so-called CM relation, has been found for many rich galaxy clusters (Bower et al. 1992, and references therein). For early-type galaxies in a cluster, the brighter galaxies tend to have colors redder than the fainter galaxies do. This relation can be used for verifying the membership selection of the early-type galaxies within the BATC field (Yuan et al. 2001). In order to select the member early-type galaxies, we take the Hubble types of the best-fit SED templates as morphology classifications. Figure 9 presents the correlation between the color index $u' - p$ versus h-magnitude for the known and new early-type member candidates. The open circles denote newly selected early-types and the filled circles denote the known early-types. The solid line denotes the least-square fit for the linear relation with 65 known early-type galaxies:$u' - p = -0.26(\pm0.04)h + 7.53(\pm0.70)$. The dashed lines represent $\pm1\sigma$ deviation. Taking all photometric early-types into account, an horizontal line, $u' - p = 3.15$, seems to be also a good model of the red sequence, which means red galaxies in A2589 might have a typical $u' - p$ color. **It is noticed that the good CM relation might be artificial because red galaxies are likely to be classified as early-types by the HYPERZ code.**

As shown in Figure 9, most of early-type candidates agree with the CM correlation derived by the known early-type galaxies. There are 8 early-type candidates with colors beyond the 2σ deviation of intercept that have probably been misclassified. Taking only the templates of late-type galaxies, we apply the SED-fitting procedures again on these 8 candidates. As a result, 4 of them are found to have the best-fit template SEDs of Sa galaxies with redshifts between 0.016 and 0.062, and they are therefore regarded as late-type member galaxies. The remaining 4 candidates are excluded from the list of member galaxies.

Finally, we obtain a list of 106 ($= 110 - 4$) newly-selected member galaxies. Combined with the 68 spectroscopically confirmed member galaxies, we have obtained an enlarged sample of 174 member galaxies which includes 130 early-type galaxies and 44 late-type galaxies. We refer to this sample as “sample II” hereafter. Table 3 presents the catalog of SED information for the 106 newly-selected members, including the ID number, the SDSS-given celestial coordinate in degrees, photometric redshift, morphological class of the best-fit template, and combined SED information. The classification indices in a range from 1 to 7 are defined to denote E, S0, Sa, Sb, Sc, Sd and Im galaxies, respectively. The magnitude of 99.00 means non-detection in the specified band.

4. Physical Properties of Regular Cluster A2589

4.1. Spatial Distribution

The X-ray images obtained in the ROSAT (Buote & Tsai 1996) and $Chandra$ (Buote & Lewis 2004) observations support a picture that A2589 has a smooth X-ray morphology and no sign of ongoing merger. The optical map of cluster galaxies also shows no evidence of subclusters in A2589 (Beers et al. 1991). The projected distribution of the 68 member galaxies in sample I is given in Figure 10(a). In order to show the overall morphology of galaxy two-dimension distribution, we superpose the contour map of the surface density that has been smoothed by a Gaussian window with σ =3′. It is easy to find that A2589 concentration is rather compact: more than 50% of bright known member galaxies are located within a small circular region with $r = 0.5$ Mpc. The contour profiles tend to be more asymmetric at larger radius, but no detached clumps (i.e. substructures) of galaxies are detected. Figure 10(a) shows an elongation along the north-south direction, which seems to agree with the X-ray brightness profile and the orientation of central cD galaxy.

For the 174 member galaxies in sample II, the projected distribution is also given in Figure 10(b). We superpose the contour map of the spatial distribution that has been smoothed by a Gaussian window with $\sigma = 4'$. The filled circles denote the 68 member galaxies with known spectroscopic redshifts, and the open circles denote the 103 newly-selected member galaxies. Though the sample size increases by nearly 150%, the profile of surface density does not change a lot, with the same orientation and shape in central region, and no discrete substructure is detectable at a low surface density level of 0.14 arcmin^{-2}.

4.2. Localized Velocity Structure

Projected distribution of galaxies appears smooth and relaxed, which might be due to projection effect. A true substructure should be verified in the line-of-sight velocity space. The κ-test has been commonly used for this purpose, which was developed by Colless & Dunn (1996) for quantifying localized variation

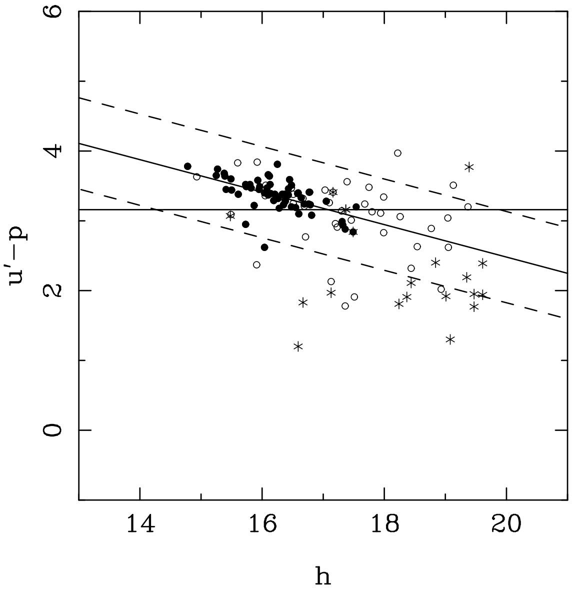

Fig. 9.— Color-magnitude relation for 130 early-type galaxies in A2589, including 65 early-type galaxies with known spectroscopic redshifts (*filled circles*) and 65 newly-selected member candidates (*open circles*). The 44 late-type member galaxies are also plotted (*stars*). A linear fit is given to the 65 spectroscopically-confirmed early-type members, and the dash lines correspond to the ±1σ of the linear fitting.

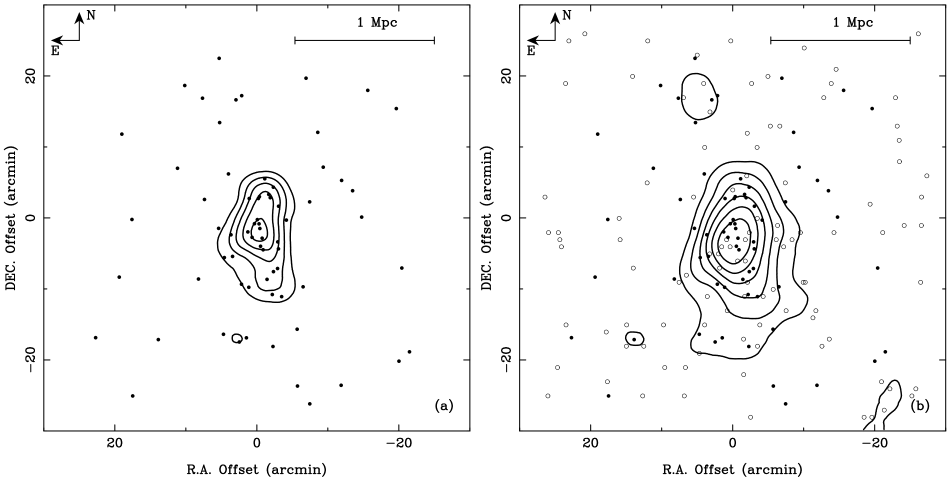

Fig. 10.— Left: Spatial distribution for 68 spectroscopic member galaxies of A2589 in sample I. The contour map of the surface density using the smoothing Gaussian window $\sigma = 3'$ is used. Right: Spatial distribution for 171 member galaxies in sample II. The smoothing Gaussian window is σ=4′. For both panels, the contour levels are 0.09, 0.14, 0.19, 0.24, 0.29, and 0.34 arcmin^{-2}, respectively.

in velocity distribution. A test statistic κ_n is defined to characterize the local deviation on the scale of the groups of *n* nearest neighbors based on the Kolmogorov-Smirnov test (KS-test). Larger κ_n means greater possibility that the local velocity distribution differs from the whole distribution. The probability that κ_n is larger than the observed value, P($\kappa_n > \kappa_n^{obs}$), can be estimated by Monte Carlo simulations by randomly shuffling velocities. Table 4 gives the results of the κ-test for samples I and II, and the 10^3 simulations are made for all cases. A limit of P($\kappa_n > \kappa_n^{obs}$) for substructure detection is 5%, corresponding to the 2σ significance. For the 68 member galaxies in sample I, the probability P($\kappa_n > \kappa_n^{obs}$) is found to be about 80% (much more than the limit 5%) in a wide range of neighbor size, which strongly supports non-detection of substructure. Even for the enlarged sample of 174 member galaxies, the probability P($\kappa_n > \kappa_n^{obs}$) is still over 16% which is greater by two times than the limit 5%. No substructures are detected at more than 2σ significance on the basis of sample II.

Figure 11 shows the bubble plots of the localized velocity variation, using the neighbor size $n = 9$ for both samples. The bubble size for each galaxies is proportional to $-$log[P$_{\rm KS}$(D>D$_{\rm obs}$)]. Therefore, the larger bubbles indicate a greater difference between local and overall velocity distributions. There is no prominent bubble clustering in the core region of A2589. For the 68 spectroscopic galaxies in sample I, the central bubbles are very tiny, indicating that the local velocity distribution is in well accordance with the overall one. Even for the enlarged sample II, bubble clustering at center is still neglectable. A close comparison between the projected distribution (in Figure 10) and bubble plot (in Figure 11) shows that A2589 is a well-relaxed cluster with no dynamic substructures detected both in 2-d mapping and in radial velocity space.

An elongation along the north-south direction has been unveiled in Figure 10. To make certain of whether there exists a substructure located about 10 arcmin south to the main concentration, we further apply

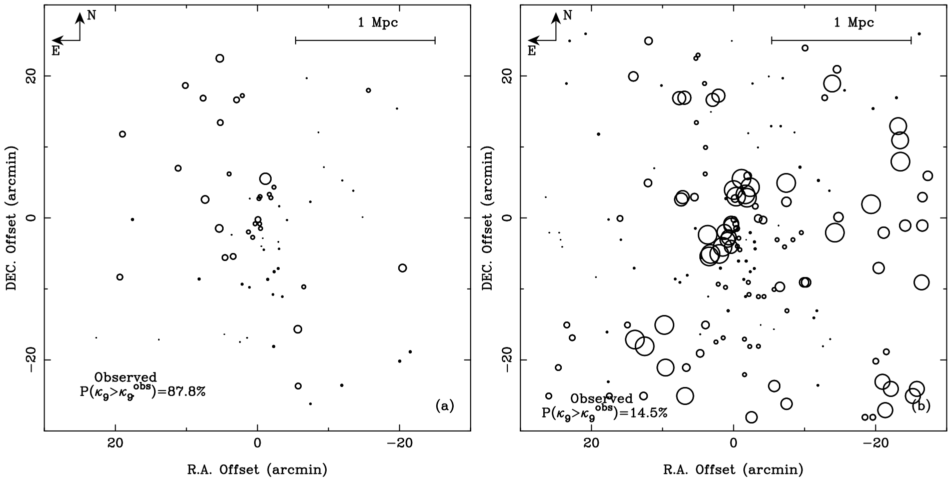

Fig. 11.— (a) Bubble plot showing the localized variation for groups of the 9 nearest neighbors for (a) 68 galaxies in sample I; (b) 174 galaxies in sample II

a currently favored technique of mixture modeling, namely the KMM algorithm, to the samples I and II. The KMM is a maximum-likelihood algorithm which assigns objects into groups and assesses the improvement in fitting a multi-group over a single group model (Ashman et al. 1994). Based on the three-dimension data (i.e., projected positions and radial velocities of member galaxies), we set the initial positions: (0.0, 0.0) for the main concentration and (-2.0, -11.0) for the possible substructure, and the initial mean velocities are 12050 $\mathrm{km\,s^{-1}}$for two clumps. The KMM algorithm gives following optimum two-group solutions: only three galaxies in sample I are assigned as the members of southern substructure, and only five galaxies in sample II are allocated to the substructure. This means the southern anormal feature in projected mapping is not a significant substructure, which supports the conclusion drawn by the κ-test that no significant dynamic substructures are found in A2589.

4.3. Luminosity Function

The luminosity function (LF) is a fundamental tool to analyze the properties of galaxies in a cluster. Usually, a Gaussian function can be used to describe the LF of bright galaxies with $i < 19^m.0$ (Binggeli et al. 1988) $N(M) \sim exp[-(M-\mu)^2/2\sigma^2]$, where μ is the characteristic absolute magnitude, and σ is the dispersion. For the faint galaxies with $i > 19^m.0$, a Schechter function is needed to give a better fit (Schechter 1976): $N(M) = \phi^*[10^{-0.4(M-M^*)}]^{(\alpha+1)}e^{-10^{-0.4(M-M^*)}}$, where ϕ^*, M^*, and α are the normalization parameter, the characteristic absolute magnitude, and the slope at faint end, respectively. For the cluster galaxies, a single Schechter function can not give a perfect description for the LFs (Driver et al. 1994; Mohr et al. 1996; Trentham & Tully 2002; Yang et al. 2004). Ferguson & Sandage (1991) performed a LF fitting with these two functions.

For comparing with previous results, the BATC magnitudes are converted into the conventional Kron-

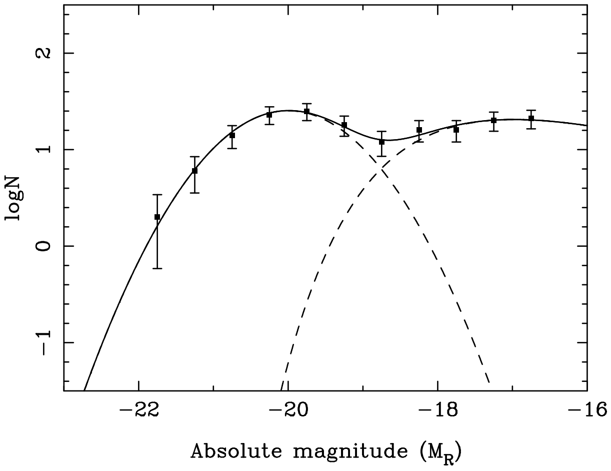

Fig. 12.— Observed luminosity function of R band. The dashed lines indicate the components of the Gauss and Schechter function, the solid lines are their sum.

Cousins magnitudes via the equations in Zhou et al. (2003). The M_R magnitudes in sample II cover a range from -22.0 to -16.5 mag, and a turn-off point at $M_R = -18.75$ is found in magnitude distribution. We use the combination of above two functions to describe the LFs of galaxies in A2589: a Gaussian function for the bright galaxies, and a Schechter function for the faint galaxies. The fitting results in a Gaussian function with $\mu = -20.0^{+0.02}_{-0.18}$, σ=$-1.34^{+0.02}_{-0.02}$, and a Schechter function with $M^* = -17.8^{+0.35}_{-0.01}$, $\alpha = -0.53^{+0.20}_{-0.04}$. The combination of two functions gives a good description for the LFs of A2589 (see Figure 12).

Though the uncertainty in member selection might be larger for faint galaxies, the LF peak at $M_R \sim -20$ and dip at $M_R \sim -19$ might be real because the BATC photometry is capable for detecting the galaxies brighter than 19.5 mag. With the clear peak at $M_R \sim -20$, the bright part LF of A2589 looks similar with the LF of rich clusters, which have a bump in bright part (Biviano et al. 1995). Our turn-off magnitude $M_R = -18.75$ is similar to the LFs in A963 (Driver et al. 1994), Coma (Thompson & Gregory 1993), and A2554 (Smith et al. 1997). For the LF slope at faint parameter α, A2589 has a flat slope than many rich clusters, which might be due to the incompleteness in selection of faint members.

Following the definition of dwarf-to-giant ratio in Driver et al. (1998), we define the faint-to-bright ratio (FBR) as the count ratio of faint galaxies to bright galaxies, FBR=$\sum N(M_R > -18.75) / \sum N(M_R < -18.75)$. The overall FBR is about 0.84. It is found that the FBR varies with clustercentric radius: $FBR = 0.44$ in central region ($R \leq$0.5Mpc), and $FBR = 1.23$ in outer region ($R >$ 0.5Mpc). The increasing tendency of the FBR along radial distance is presented in Figure 13. Obviously, the LF faint end is dominated by faint/dwarf galaxies, which can be interpreted by the 'dwarf population density' relation (Phillipps et al. 1998): dwarves are more common in the low density environment. This segregation may originate from initial conditions of formation of dwarf galaxies, where low luminosity galaxies are only now in-falling into clusters (Croton et al. 2005), or the galaxies may have suffered the processes internal to clusters, such as tidal disruption and galaxy harassment (Mastropietro et al. 2005; Aguerri 2004, 2005), consequently dimmed.

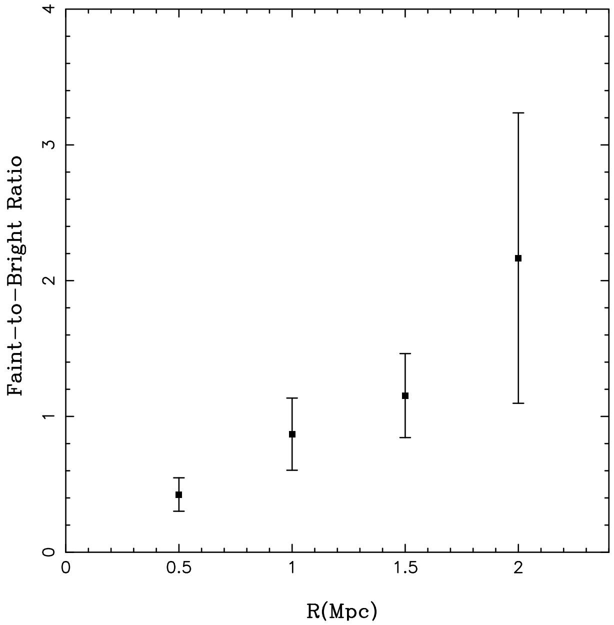

Fig. 13.— The faint-to-bright ratio (FBR) as a function of clustercentric distance of A2589. The mean FBRs are computed in annuli of 0.5Mpc width .

4.4. Star Formation Properties of Cluster Galaxies

The star formation histories of the member galaxies can provide important clues for understanding the evolution of their host cluster. For a cluster galaxy, both the cluster-scale gravity environment and the galaxy-scale interaction may have influenced the physical processes concerning star formation. Therefore, it is interesting to observe the systematic tendency of the star formation properties for the galaxies in a cluster.

With an evolution synthesis model, PEGASE (version 2.0, Fioc & Rocca-Volmerange (1997, 1999)), the star formation properties of A2589 are investigated. We assume a Salpeter (1955) initial mass function (IMF) and a star formation rate (SFR) in exponentially decreasing form, $SFR(t) \propto e^{-t/\tau}$, where the time scale τ ranges from 0.5 to 30.0 Gyr. To avoid the degeneracy between age and metallicity in the model, we use the same age of 12.86 Gyr for all the member galaxies in A2589, responding to the age of the first generation stars at z_c =0.0414. A zero initial metallicity of interstellar medium (ISM) is assumed. Firstly, a series of rest-frame modeled spectra at z=0 with various star formation histories are generated by running the PEGASE code. Then we shift them to the observer's frame for a given redshift, and then convolve with the transmission functions of the BATC and SDSS filters. As a result, we obtain the template SED library containing the BATC and SDSS photometric bands.

Based on the template SED library, we search for the minimal χ^2 fit of the observed SEDs of 68 bright member galaxies with known spectroscopic redshifts. The SFR time scale (τ), mean ISM metallicity ($\mathrm{Z_{ISM}}$), and the mean stellar age ($t_\star$) weighted by mass and light can be achieved.

Figure 14 shows the star formation properties as a function of the projected radius (*R*) for 68 member galaxies in sample I. The dash lines denote the best linear fitting results. Panel (a) shows that the SFR time scale is shorter in the inner region than that in the outer region. This result agrees with the morphology-density relation pointed out by Dressler (1980), which can be well explained in the context of hierarchical cosmological scenario (Poggianti 2004). Panel (b) presents that the outlier galaxies have higher probability to have a lower metallicity, which is consistent with the pictures that more massive galaxies form fractionally more stars in a Hubble time than the low-mass counterparts, and metals are selectively lost from the faint galaxies with shallow potential wells via galactic winds (Tremonti et al. 2004). Panels (c) and (d) show that the galaxies in the core region tend to possess older stellar population with longer mean stellar ages weighted by either mass or light. Comparison between panels (c) and (d) shows that the gradient of the light-weighted stellar age is steeper. After the evolution of galaxies, stellar mass are dominated by old stellar population with dimmed light. On the other hand, current star formation rate in a cluster is mainly contributed by the late-type galaxies in the outer region, and younger stellar population has a greater weight in mean age calculation. It is reasonable that the stellar ages weighted by bolometric luminosity tend to be younger for the outlier galaxies.

Figure 15 gives the SFR time scale τ and the ISM metallicities as a function of absolute magnitude (M_R). The high luminosity galaxies tend to have shorter time scales. For the bright and massive cluster galaxies in the core region of A2589, their star formation activities might have been reduced by many different physical process via environmental effects, such as galaxy-galaxy interaction, harassment, gas stripping, strangulation (Poggianti 2004; Yuan et al. 2005), which results in a short time scale of star formation.

5. Summary

We present our multicolor optical photometry for the nearby regular cluster of galaxies A2589, based on the BATC 15-intermediate bands system and SDSS photometric data. The SEDs in 15 bands are obtained for more than 5000 sources detected from ~1 deg^2 of the BATC images. After cross-identifying the BATC sources with the SDSS photometric catalog, 1199 galaxies are extracted. An interpolation method is performed to make zero-point correction, the combined 20-band SEDs for 1199 galaxies are archived. Then, a photometric redshift technique and the CM relation of early-type galaxies are applied to select fainter member galaxies. As a result, 106 galaxies are selected as the faint member galaxies. Combining 68 member galaxies with known spectroscopic redshifts (i.e., sample I) , we obtain an enlarged sample of 174 member galaxies (i.e., sample II).

The projected distribution shows no prominent clumps. The contour of surface density shows an north-south elongation, which agrees with the X-ray brightness profile and the orientation of central cD galaxy, NGC 7647. Subsequential κ-test also indicates no substructure in the galaxy cluster A2589, which agrees with the X-ray images by $ROSTAT$ (Buote & Tsai 1996) and *Chandra* (Buote & Lewis 2004). Our conclusion is that A2589 is a well-virialized and relaxed system.

The luminosity function of member galaxies in A2589 shows a peak at $M_R \sim -20.0$ and a dip at

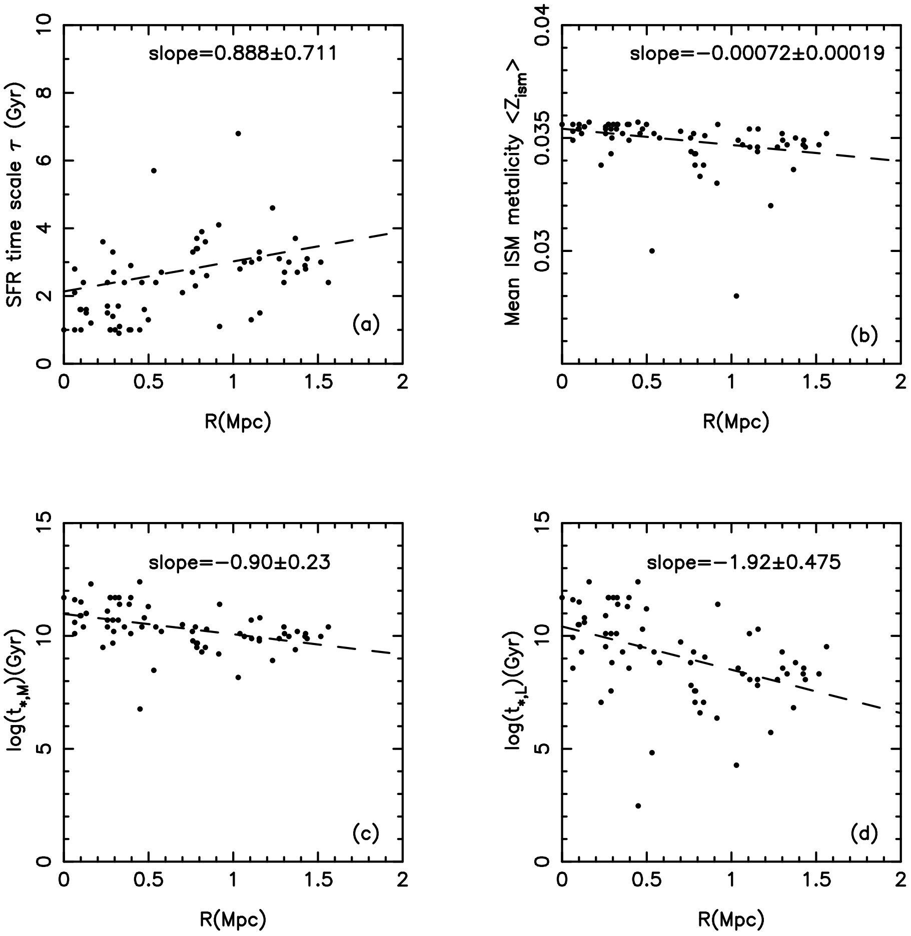

Fig. 14.— Star formation properties for the galaxies with known z_{sp} in A 2589 as a function of the project radius R. The star formation properties are the SFR time scale τ, mean ISM metallicity, and the mean stellar ages weighted by mass and light.

$M_R \sim -19.0$. Compared with other clusters, the turn-off point seems to be independent on the richness and dynamic stage. The faint-bright-ratio (FBR) increases monotonously along clustercentric distance, indicating that the faint and dwarf galaxies tend to be located in the outer region of cluster.

The star formation properties of cluster galaxies unveils an environmental influence on evolution of A2589. Bright and massive galaxies in the core region are found to have shorter SFR time scales, longer mean stellar ages, and higher mean ISM metallicities, while the outlier galaxies are likely to have smaller stellar ages, and longer SFR time scales. These results can be well interpreted by the existing correlations, such as the morphology-density relation, the luminosity-metallicity relation, and the mass-metallicity relation.

We thank the anonymous referee for his/her invaluable comments and suggestions. This work was

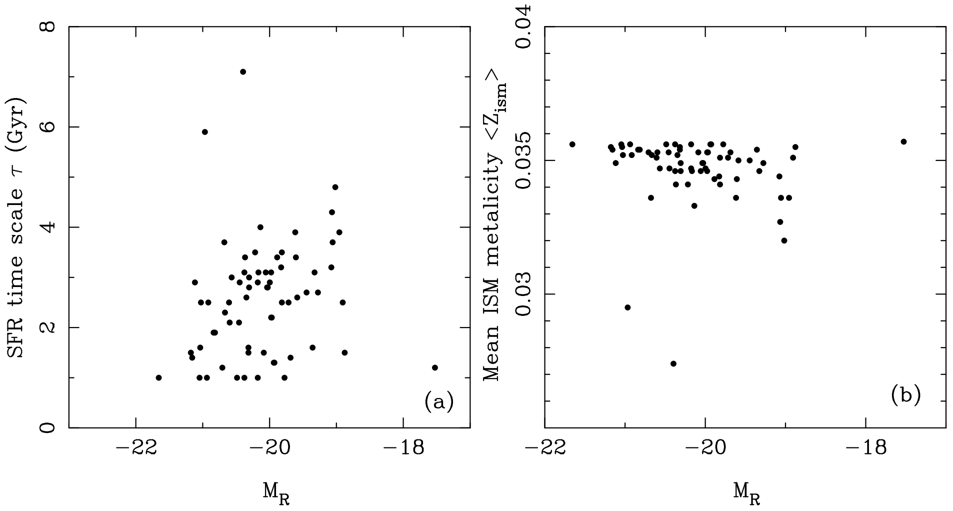

Fig. 15.— The SFR time scale τ and mean ISM metallicities for the galaxies with known z_{sp} in A2589 as the function of magnitude in R band.

funded by the National Natural Science Foundation of China (NSFC) (Grant Nos. 10778618, 10633020, 10873016, 10603006, and 10803007), and by the National Basic Research Program of China (973 Program) (Grant No. 2007CB815403). This research has made use of the NED, which is operated by the Jet Propulsion Laboratory, California Institute of Technology, under contract with the National Aeronautics and Space Administration. We would like to thank Prof. Kong, X. and Cheng, F.-Z. at the University of Science and Technology of China for the valuable discussion.

REFERENCES

Abell, G. O. 1958, ApJS, 3, 211

Adami, C., et al. 2009, A&A, 507, 1225

Aguerri, J. A. L., Iglesias-Paramo, J., Vilchez, J. M., & Muñoz-Tuñón, C. 2004, AJ, 127, 1344

Aguerri, J. A. L., Gerhard, O. E., Arnaboldi, M., Napolitano, N. R., Castro-Rodriguez, N., & Freeman, K. C. 2005, AJ, 129, 2585

Allen, D. A. 1976, MNRAS, 174, 29P

Arnouts, S., et al. 1999, MNRAS, 310, 540

Ashman, K. M., Bird, C. M., & Zept, S. E. 1994, AJ, 108, 2348

Bahcall, N. A. 1996, arXiv:astro-ph/9612046

Bauer, F. E., Condon, J. J., Thuan, T. X., & Broderick, J. J. 2000, ApJS, 129, 547

Bautz, L. P., & Morgan, W. W. 1970, ApJ, 162, L149

Beers, T. C., Flynn, K., & Gebhardt, K. 1990, AJ, 100, 32

Beers, T. C., Gebhardt, K., Forman, W., Huchra, J. P., & Jones, C. 1991, AJ, 102, 1581

Bekki, K. 2001, Ap&SS, 276, 1033

Binggeli, B., Sandage, A., & Tammann, G. A. 1988, ARA&A, 26, 509

Biviano, A., Durret, F., Gerbal, D., Le Fevre, O., Lobo, C., Mazure, A., & Slezak, E. 1995, A&A, 297, 610

Bolzonella, M., Miralles, J.-M., & Pelló, R. 2000, A&A, 363, 476

Bothun, G. D., & Schombert, J. M. 1988, ApJ, 335, 617

Bower, R. G., Lucey, J. R., & Ellis, R. S. 1992, MNRAS, 254, 589

Bower, T. C., Balogh, M. L., 2004, in Clusters of Galaxies: probe of cosmological structure and galaxy evolution, p.326. eds. J. S. Mulchaey, A. Dressler, A. Oemler, Cambridge University press

Bruzual A., G., & Charlot, S. 1993, ApJ, 405, 538

Buote, D. A., & Lewis, A. D. 2004, ApJ, 604, 116

Buote, D. A., & Tsai, J. C. 1996, ApJ, 458, 27

Burns, J. O., Rhee, G., Owen, F. N., & Pinkney, J. 1994, ApJ, 423, 94

Capelato, H. V., Mazure, A., Proust, D., Vanderriest, C., Lemonnier, J. P., & Sodre, L., Jr. 1991, A&AS, 90, 355

Cen, R., & Ostriker, J. 1994, ApJ, 429, 4

Colless, M., & Dunn, A. M. 1996, ApJ, 458, 435

Croton, D. J., et al. 2005, MNRAS, 356, 1155

David, L. P., Jones, C., & Forman, W. 1996, ApJ, 473, 692

Dressler, A. 1980, ApJS, 42, 565

Driver, S. P., Phillipps, S., Davies, J. I., Morgan, I., & Disney, M. J. 1994, MNRAS, 268, 393

Driver, S. P., Couch, W. J., & Phillipps, S. 1998, MNRAS, 301, 369

Evrard, A. E. 1989, ApJ, 341, L71

Fan, X., et al. 1996, AJ, 112, 628

Ferguson, H. C., & Sandage, A. 1991, AJ, 101, 765

Fioc, M., & Rocca-Volmerange, B. 1997, A&A, 326, 950

Fioc, M., & Rocca-Volmerange, B. 1999, A&A, 351, 869

Forman, W., & Jones, C. 1982, ARA&A, 20, 547

Frenk, C. S., White, S. D. M., Efstathiou, G., & Davis, M. 1990, ApJ, 351, 10

Frenk, C. S., et al. 1996, ApJ, 472, 146

Furusawa, H., Shimasaku, K., Doi, M., & Okamura, S. 2000, ApJ, 534, 624

Gunn, J. E., & Stryker, L. L. 1983, ApJS, 52, 121

Haynes, M. P., Giovanelli, R., Herter, T., Vogt, N. P., Freudling, W., Maia, M. A. G., Salzer, J. J., & Wegner, G. 1997, AJ, 113, 1197

Henry, J. P., & Briel, U. G. 1993, Advances in Space Research, 13, 191

Jenkner, H., Lasker, B. M., Sturch, C. R., McLean, B. J., Shara, M. M., & Russel, J. L. 1990, AJ, 99, 2082

Kambas, A., Davies, J. I., Smith, R. M., Bianchi, S., & Haynes, J. A. 2000, AJ, 120, 1316

Lanzetta, K. M., Yahil, A., & Fernández-Soto, A. 1996, Nature, 381, 759

Lupton, R. 2005, http://www.sdss.org/dr5/algorithms/sdssUBVRITransform.html

Mastropietro, C., Moore, B., Mayer, L., Debattista, V. P., Piffaretti, R., & Stadel, J. 2005, MNRAS, 364, 607

McCarthy, I. G., Balogh, M. L., Babul, A., Poole, G. B., & Horner, D. J. 2004, ApJ, 613, 811

Mihos, J. C., 2004, in Cluster of Galaxies: probe of cosmological structure and galaxy evolution, p.278, eds. J. S. Mulchaey, A. Dressler, A. Oemler, Cambridge University press

Mohr, J. J., Geller, M. J., Fabricant, D. G., Wegner, G., Thorstensen, J., & Richstone, D. O. 1996, ApJ, 470, 724

Moore, B., Lake, G., & Katz, N. 1998, ApJ, 495, 139

Navarro, J. F., & White, S. D. M. 1994, MNRAS, 267, 401

Neumann, D. M., Lumb, D. H., Pratt, G. W., & Briel, U. G. 2003, A&A, 400, 811

Phillipps, S., Driver, S. P., Couch, W. J., & Smith, R. M. 1998, ApJ, 498, L119

Poggianti, B. 2004, Proceedings of “Baryons in Dark Matter Halos”. Novigrad Croatia, 5-9 Oct 2004. Editors: R. Dettmar, U. Klein, P. Salucci. Published by SISSA, Proceeding of Science, p.104.1

Quilis, V., Moore, B., & Bower, R. 2000, Science, 288, 1617

Rhee, G. F. R. N., & Latour, H. J. 1991, A&A, 243, 38

Roettiger, K., Burns, J. O., & Loken, C. 1996, ApJ, 473, 651

Salpeter, E. E. 1955, ApJ, 121, 161

Salvador-Sole, E., Gonzalez-Casado, G., & Solanes, J. M. 1993, ApJ, 410, 1

Sarazin, C. L., O’Connell, R. W., & McNamara, B. R. 1992, ApJ, 397, L31

Schechter, P. 1976, ApJ, 203, 297

Smith, R. M., Driver, S. P., & Phillipps, S. 1997, MNRAS, 287, 415

Smith, R. J., et al. 2004, AJ, 128, 1558

Stetson, P. B. 1987, PASP, 99, 191

Struble, M. F., & Rood, H. J. 1999, ApJS, 125, 35

Thompson, L. A., & Gregory, S. A. 1993, AJ, 106, 2197

Tremonti, C. A., et al. 2004, ApJ, 613, 898

Trentham, N., & Tully, R. B. 2002, MNRAS, 335, 712

Wegner, G., Colless, M., Saglia, R. P., McMahan, R. K., Davies, R. L., Burstein, D., & Baggley, G. 1999, MNRAS, 305, 259

White, S. D. M., Briel, U. G., & Henry, J. P. 1993, MNRAS, 261, L8

Xia, L., et al. 2002, PASP, 114, 1349

Yan, H., et al. 2000, PASP, 112, 691

Yang, Y, et al. 2004, AJ, 600, 141

Yuan, Q., et al. 2001 AJ, 122, 1718

Yuan, Q., Zhou, X., & Jiang, J. 2003, ApJS, 149, 53

Yuan, Q., Zhao, L., & Yang, Y., et al. 2005, AJ, 130, 255

Zhang, L., Yuan, Q., & Zhou, X., et al. 2010, RAA, 10,1

Zhou, X., et al. 1999, PASP, 111, 909

Zhou, X., et al. 2001, Chinese J. Astron. Astrophys., 1, 372

Zhou, X., et al. 2003, A&A, 397, 361

This preprint was prepared with the AAS LaTeX macros v5.2.

Table 3: Catalog of 106 Newly-selected Candidates of Member Galaxies in A2589

No.	R.A.	Decl.	$z_{\rm ph}$	T	a	b	c	d	e	f	g	h	i	j	k	m	n	o	p	u'	g'	r'	i'	z'
1	350.52581787	16.92402267	0.048	1	19.97	20.47	19.79	19.14	18.77	18.73	18.37	18.22	18.02	17.91	99.00	17.92	17.96	17.65	17.31	21.28	19.12	17.71	17.96	17.71
2	350.53906250	16.87807274	0.056	2	18.81	18.14	17.90	17.46	17.11	16.89	16.64	16.51	16.29	16.21	16.21	16.02	15.90	15.83	15.65	18.90	17.37	16.55	16.12	15.81
3	350.53964233	16.80180168	0.025	7	19.67	18.74	18.76	18.87	18.76	18.78	18.73	18.59	18.59	18.46	18.61	18.57	18.41	18.95	18.30	20.28	18.78	18.83	18.64	17.51
4	350.54162598	16.67333031	0.033	3	17.46	17.12	16.89	16.80	16.70	16.64	16.63	16.59	16.27	16.29	16.56	16.42	16.43	16.32	16.44	17.64	16.83	16.59	16.38	16.31
5	350.54580688	17.26466942	0.044	1	18.43	18.17	17.35	16.98	16.61	16.48	16.12	16.05	15.82	15.84	15.83	15.58	15.48	15.41	15.29	18.65	16.88	16.08	15.71	15.40
6	350.55383301	16.42631340	0.030	4	99.00	17.89	17.36	17.30	17.17	17.09	17.01	16.94	16.64	16.68	16.78	16.67	16.62	16.51	16.42	18.28	17.38	16.91	16.72	16.53
7	350.56356812	16.40281296	0.057	1	99.00	19.14	18.76	18.34	17.92	17.67	17.50	17.38	17.12	17.11	17.02	16.83	16.74	16.65	16.59	20.31	18.26	17.32	16.91	16.70
8	350.58166504	16.80896950	0.046	3	99.00	19.30	19.08	19.27	19.09	19.00	18.84	18.76	18.47	18.42	18.83	18.39	18.20	17.90	18.04	27.70	19.21	18.70	18.44	18.47
9	350.59280396	16.95937729	0.027	2	21.58	20.38	20.05	20.26	19.60	19.54	19.30	19.37	19.17	19.00	19.23	19.09	18.62	18.73	18.58	21.78	19.96	19.39	19.01	18.84
10	350.59347534	17.01498795	0.061	1	18.23	18.19	17.76	17.08	16.59	16.36	16.04	15.92	15.67	15.61	15.56	15.34	15.28	15.19	15.02	18.86	16.91	15.98	15.53	15.21
11	350.59823608	17.03547859	0.060	4	18.41	18.12	17.76	17.67	17.47	17.34	17.20	17.13	17.01	16.74	17.01	16.81	16.77	16.76	16.68	18.65	17.63	17.17	16.84	16.73
12	350.60241699	17.10379982	0.049	1	19.14	18.44	17.81	17.45	17.06	16.95	16.61	16.51	16.30	16.28	16.26	16.04	15.95	15.88	15.78	19.16	17.34	16.55	16.17	15.87
13	350.61746216	16.42463112	0.023	1	99.00	20.87	23.37	21.43	20.31	20.35	19.81	19.77	19.44	19.95	19.31	19.61	19.63	18.89	19.21	21.89	20.76	19.95	19.44	19.11
14	350.63101196	16.37726974	0.048	1	99.00	20.15	20.43	18.97	19.07	19.17	18.84	18.77	18.34	18.68	99.00	18.76	18.60	18.93	18.08	21.33	20.02	18.94	18.48	18.07
15	350.63424683	16.78801537	0.017	1	19.89	19.24	20.16	19.33	18.95	18.87	18.54	18.42	18.16	18.04	17.96	17.83	17.70	17.72	17.48	20.93	19.24	18.43	17.92	17.62
16	350.63787842	16.44768906	0.034	1	99.00	18.21	18.07	17.93	17.80	17.77	17.71	17.68	17.49	17.48	17.61	17.59	17.45	17.26	17.38	19.08	17.91	17.62	17.52	17.63
17	350.66183472	16.35647392	0.053	1	99.00	18.22	19.08	18.75	18.23	18.05	17.84	17.77	17.48	17.38	17.45	17.31	17.12	17.09	17.09	20.48	18.57	17.74	17.35	17.08
18	350.66513062	16.86167526	0.024	3	17.74	17.16	16.55	16.31	16.00	15.89	15.59	15.48	15.21	15.20	15.11	15.00	14.85	14.73	14.68	17.75	16.24	15.47	15.06	14.74
19	350.68112183	16.36630630	0.037	1	99.00	18.48	18.64	18.42	18.31	18.25	18.14	18.03	17.87	17.76	18.11	17.87	17.75	17.87	17.70	19.81	18.33	18.05	17.81	17.88
20	350.74844360	17.16712379	0.043	1	18.98	18.49	17.84	17.45	17.04	16.91	16.57	16.48	16.28	16.25	16.19	15.97	15.91	15.79	15.74	19.21	17.31	16.51	16.12	15.82
21	350.75390625	16.79937553	0.024	2	19.40	17.97	17.70	17.55	17.37	17.32	17.22	17.13	16.90	16.86	16.93	16.86	16.79	16.66	16.61	18.74	17.49	17.09	16.85	16.73
22	350.75997925	17.14521217	0.039	3	19.86	19.90	19.73	20.21	19.71	19.59	19.28	19.20	18.92	19.17	18.94	18.87	18.52	18.41	18.72	21.14	19.85	19.22	18.91	18.76
23	350.76577759	16.54315758	0.049	1	20.30	20.17	20.00	19.01	18.83	18.77	18.41	18.44	18.28	18.27	18.29	18.16	18.24	18.04	18.40	20.72	19.24	18.01	18.31	18.09
24	350.77868652	17.10724640	0.024	1	20.60	19.35	19.24	19.50	19.68	19.58	19.74	19.38	19.15	19.26	19.36	19.24	18.96	18.83	18.27	20.94	19.65	19.26	19.09	19.02
25	350.78274536	16.53175163	0.044	1	18.69	17.89	16.86	15.96	15.78	15.60	15.09	14.93	14.69	14.55	14.42	14.30	14.22	14.11	14.08	17.71	15.79	14.75	14.54	15.16
26	350.79830933	16.60096359	0.043	1	21.28	20.15	19.27	19.26	19.10	19.09	18.99	18.93	18.85	18.82	19.27	18.91	18.58	18.54	19.00	21.02	19.26	18.85	18.62	18.75
27	350.80563354	16.58921432	0.031	1	18.68	18.03	17.76	17.80	17.64	17.56	17.55	17.48	17.24	17.24	17.33	17.26	17.14	17.26	17.15	18.95	17.79	17.48	17.28	17.13
28	350.82449341	16.66783524	0.049	1	20.62	19.83	19.37	19.16	18.85	18.71	99.00	18.54	18.33	18.26	18.43	18.27	18.22	18.15	17.70	20.33	19.10	18.59	18.35	18.10
29	350.82653809	17.22652817	0.039	2	18.35	18.39	17.60	17.49	17.24	17.10	16.78	16.71	16.49	16.47	16.45	16.25	16.18	16.08	16.02	18.79	17.39	16.71	16.34	16.12
30	350.82934570	16.66695786	0.042	1	99.00	19.18	22.12	21.04	20.26	19.84	19.63	19.42	19.39	19.38	19.75	19.36	18.77	18.94	18.26	21.60	20.64	19.74	19.32	18.99
31	350.83618164	16.79516220	0.044	2	18.94	18.48	18.03	17.98	17.76	17.69	17.57	17.51	17.31	17.34	17.34	17.24	17.16	17.15	17.20	19.11	17.95	17.53	17.28	17.10
32	350.85662842	16.77861404	0.026	4	19.63	19.39	19.17	19.20	19.10	19.08	18.82	18.77	18.67	18.67	18.45	18.57	18.13	18.28	18.15	20.28	19.18	18.71	18.46	18.30
33	350.87145996	16.61509132	0.030	1	99.00	21.13	21.10	19.81	19.79	19.72	19.44	19.09	18.92	19.01	19.11	19.02	18.78	18.99	18.28	21.46	19.95	19.30	18.94	18.74
34	350.87319946	16.90993500	0.048	5	18.74	17.81	17.28	17.19	17.00	16.93	16.74	16.67	16.38	16.39	16.55	16.40	16.33	16.26	16.18	18.01	17.12	16.71	16.53	16.03
35	350.87722778	16.76000595	0.031	1	20.83	19.47	18.77	18.22	17.91	17.83	17.53	17.46	17.20	17.12	17.13	17.00	16.84	16.76	16.81	19.82	18.19	17.42	17.07	16.79
36	350.88580322	17.04202461	0.059	3	99.00	20.15	19.62	19.63	19.33	19.19	18.86	18.66	18.42	18.42	18.61	18.18	18.24	18.16	18.08	21.35	19.19	18.80	18.40	22.37
37	350.89169312	16.81429672	0.050	3	20.64	99.00	19.21	19.50	19.07	18.98	18.75	18.59	18.03	18.36	18.32	18.21	18.01	18.14	17.76	20.76	19.36	18.63	18.28	18.07
38	350.89550781	16.77338600	0.023	1	19.77	19.65	18.79	18.77	18.44	18.39	18.15	17.99	17.82	17.80	17.67	17.67	17.49	17.35	17.53	20.36	18.68	17.97	17.63	17.39
39	350.90295410	16.65809059	0.034	1	19.60	18.60	18.01	17.57	17.16	17.07	16.79	16.69	16.48	16.47	16.41	16.25	16.10	16.07	15.95	19.16	17.46	16.70	16.34	16.04
40	350.90997314	17.03512764	0.044	4	20.55	19.23	20.50	20.07	19.66	19.58	19.49	19.47	19.30	19.37	19.41	19.05	18.89	18.43	19.26	21.03	19.95	19.41	19.07	18.88
41	350.91564941	17.15081024	0.024	4	99.00	19.85	19.81	19.91	19.96	19.89	19.78	19.61	19.29	19.39	19.48	19.46	19.15	19.57	18.51	20.45	20.02	19.47	19.14	20.33
42	350.92758179	16.63711929	0.038	1	99.00	21.10	19.45	18.70	18.50	18.36	18.15	17.99	17.71	17.69	17.66	17.54	17.33	17.31	17.10	20.44	18.71	17.91	17.54	17.35
43	350.93566895	16.57441330	0.056	1	19.92	19.62	19.04	18.54	18.12	18.04	17.80	17.68	17.42	17.34	17.40	17.20	17.10	17.16	16.93	20.17	18.46	17.69	17.34	17.03
44	350.94158936	16.53168869	0.018	1	99.00	20.07	20.71	21.04	19.87	20.02	19.49	19.44	18.90	19.61	18.81	18.88	18.96	18.52	18.77	21.69	20.28	19.41	18.99	18.63
45	350.94189453	16.83019829	0.043	1	19.53	18.82	18.11	17.73	17.31	17.21	16.91	16.78	16.57	16.51	16.53	16.30	16.17	16.04	16.02	19.43	17.59	16.75	16.35	16.08
46	350.94229126	16.98780251	0.028	4	19.98	19.84	20.99	19.90	19.57	19.54	19.20	19.47	19.32	19.30	19.21	19.18	19.03	18.43	19.84	20.88	19.91	19.34	18.95	18.75
47	350.95550537	17.13400650	0.040	1	20.20	19.64	19.98	19.63	19.49	19.50	19.22	19.04	18.86	18.90	18.90	18.62	18.50	18.74	18.44	21.48	19.73	19.14	18.78	18.45
48	350.95840454	16.35474205	0.053	1	20.36	20.85	21.16	20.08	19.73	19.67	19.17	19.66	19.24	18.83	19.62	19.04	18.93	19.11	18.84	21.15	20.14	19.62	19.16	19.02
49	350.96127319	16.79039574	0.053	2	19.94	21.01	19.55	21.15	20.47	20.73	20.44	20.40	19.45	19.56	19.72	19.51	19.46	19.79	19.08	22.11	21.00	20.14	19.80	19.44
50	350.96603394	16.67181778	0.045	1	20.55	19.06	18.82	18.18	17.82	17.72	17.45	17.30	17.11	17.09	17.03	16.85	16.75	16.66	16.79	19.93	18.12	17.32	16.95	16.64
51	350.96640015	17.02894592	0.026	3	19.82	19.08	19.00	18.88	18.63	18.58	18.36	18.37	18.24	18.14	18.20	18.16	18.15	17.83	18.14	20.05	18.76	18.53	18.06	17.97
52	350.96762085	16.92559433	0.053	1	22.61	19.19	18.74	18.29	17.92	17.81	17.47	17.39	17.20	17.23	17.07	16.92	16.85	16.77	16.68	20.24	18.25	17.09	17.09	16.80
53	350.97122192	16.77782631	0.046	1	22.02	99.00	18.92	18.75	18.30	18.23	17.96	17.80	17.69	17.48	17.53	17.41	17.28	17.15	17.14	20.27	18.62	17.81	17.42	17.17
54	350.97134399	16.73224449	0.036	3	20.68	99.00	20.16	19.77	19.69	19.56	19.49	19.35	19.41	18.94	19.12	18.96	18.85	18.66	18.91	21.10	19.82	19.28	18.95	18.81
55	350.97305298	16.64459801	0.045	3	22.17	99.00	20.97	20.47	19.80	20.08	20.28	19.58	19.32	19.46	20.45	19.37	19.84	18.82	18.59	23.03	20.17	19.60	19.32	19.23
56	350.97525024	16.46105576	0.053	1	99.00	20.26	20.66	19.56	19.05	18.75	18.52	18.39	18.17	18.07	18.15	17.90	17.71	17.54	17.92	21.26	19.35	18.37	17.96	17.63
57	350.97549438	16.53599358	0.046	1	99.00	20.10	19.03	18.94	18.59	18.47	18.19	18.08	17.90	17.80	17.79	17.66	17.53	17.48	17.54	20.27	18.81	18.10	17.75	17.50
58	350.99014282	16.72022820	0.052	1	21.11	20.54	20.19	20.41	20.04	19.83	19.66	19.26	19.25	19.02	19.64	18.89	18.71	19.04	18.41	21.44	20.16	19.42	19.12	19.03
59	351.00198364	16.89023781	0.060	2	19.89	19.15	20.41	19.69	19.18	19.08	18.74	18.83	18.55	18.87	18.73	18.31	18.27	18.25	18.29	21.27	19.50	18.81	18.47	18.25
60	351.00668335	17.24337769	0.046	7	19.61	19.78	19.50	19.50	19.58	19.54	19.48	19.29	19.32	18.99	19.80	19.10	19.53	18.56	18.72	20.64	19.50	19.32	19.09	19.51

Table 3: — *Continued.*

No.	R.A.	Decl.	$z_{\rm ph}$	T	a	b	c	d	e	f	g	h	i	j	k	m	n	o	p	u'	g'	r'	i'	z'
61	351.00845337	16.75835037	0.021	1	20.54	99.00	18.60	18.87	18.46	18.36	18.09	17.94	17.76	17.75	17.61	17.54	17.40	17.24	17.35	20.46	18.73	17.96	17.61	17.29
62	351.01538086	16.60781860	0.058	1	21.07	19.52	18.94	18.65	18.25	18.12	17.87	17.75	17.54	17.45	17.46	17.25	17.21	17.11	17.00	20.48	18.61	17.45	17.47	17.14
63	351.01727295	16.77843475	0.024	3	20.25	19.79	99.00	19.56	19.27	19.35	19.02	18.93	18.68	18.71	18.65	18.68	18.43	18.67	18.49	25.43	19.59	18.92	18.59	18.56
64	351.02890015	16.76558304	0.020	1	20.00	22.55	20.23	19.93	19.76	19.77	19.47	19.31	18.71	19.26	18.88	18.92	18.80	19.19	18.37	21.94	20.02	19.23	18.91	18.68
65	351.03451538	16.70536232	0.035	3	99.00	18.89	20.16	20.05	19.87	19.88	19.71	19.35	19.21	19.51	19.07	19.08	18.55	18.87	18.28	21.10	20.01	19.31	19.08	18.77
66	351.03710938	16.74093056	0.023	2	23.21	19.34	19.10	19.17	18.77	18.71	18.39	18.26	18.15	18.14	18.04	17.89	17.85	17.67	17.53	20.59	19.08	18.37	17.91	17.68
67	351.05773926	17.07377625	0.042	3	20.37	99.00	19.75	20.35	19.93	20.02	20.09	19.51	19.24	19.22	20.10	19.33	18.87	19.21	17.99	21.51	20.19	19.51	19.16	19.09
68	351.05862427	16.73395157	0.039	2	20.61	19.17	18.44	18.03	17.71	17.64	17.36	17.23	17.07	17.08	16.98	16.86	16.64	16.56	16.57	19.48	17.91	17.20	16.93	16.70
69	351.06436157	16.63640594	0.030	4	19.44	18.88	19.31	18.93	18.71	18.66	18.38	18.44	18.26	18.23	18.29	18.08	18.03	17.76	17.92	20.03	18.89	18.43	18.09	17.84
70	351.07086182	16.99158096	0.024	1	99.00	20.32	19.20	19.63	19.40	19.30	18.90	18.90	18.77	18.77	18.69	18.66	18.44	18.34	18.28	21.00	19.61	18.89	18.59	18.36
71	351.07095337	16.57386208	0.044	1	19.72	19.19	18.01	17.58	17.19	17.06	16.79	16.67	16.47	16.43	16.38	16.22	16.10	15.99	15.91	19.23	17.46	16.68	16.28	16.00
72	351.07333374	17.14213371	0.049	4	19.34	18.67	18.68	18.73	18.49	18.29	18.31	18.24	17.95	17.77	18.06	17.91	17.85	17.98	17.91	19.72	18.69	18.30	17.97	17.78
73	351.08377075	16.50154114	0.048	1	19.22	19.18	19.89	19.37	19.31	19.35	19.23	19.10	18.81	18.54	19.12	18.79	18.97	19.08	19.04	20.57	19.52	19.15	18.94	18.91
74	351.08947754	17.21441841	0.017	3	20.79	21.03	20.33	20.30	19.88	20.04	19.59	19.61	19.30	19.23	19.33	19.16	19.05	19.37	19.14	21.53	20.25	19.62	19.25	18.87
75	351.09808350	16.88235664	0.057	1	19.18	19.37	19.29	18.75	18.43	18.26	18.02	17.90	17.71	17.73	17.64	17.46	17.35	17.42	17.32	20.40	18.63	17.87	17.71	17.23
76	351.11566162	16.69385719	0.047	1	19.95	19.04	18.35	18.00	17.59	17.47	17.23	17.10	16.87	16.87	16.80	16.62	16.48	16.46	16.35	19.61	17.89	17.10	16.71	16.43
77	351.11795044	16.47721481	0.023	3	19.64	21.00	20.46	20.28	19.91	20.04	19.73	19.37	19.21	19.47	19.24	19.00	18.83	18.61	19.61	21.22	20.05	19.43	19.09	18.86
78	351.12063599	16.41191292	0.060	3	19.79	19.44	19.54	19.19	18.93	18.75	18.57	18.52	18.25	18.18	18.31	18.07	17.85	17.89	17.78	20.45	19.19	18.42	18.19	17.93
79	351.12286377	17.11305428	0.048	3	99.00	19.32	20.58	19.98	19.77	19.77	19.66	19.32	19.38	19.04	19.26	18.92	18.64	19.10	18.72	21.28	20.00	19.36	19.06	18.91
80	351.12655640	16.86726189	0.050	3	19.86	18.40	17.88	17.72	17.60	17.59	17.54	17.48	17.17	17.26	17.34	17.25	17.16	17.31	17.31	17.09	17.57	17.53	17.53	16.89
81	351.13357544	16.66821671	0.042	1	19.57	19.08	18.33	17.97	17.67	17.60	17.34	17.20	17.01	16.95	16.95	16.77	16.67	16.59	16.54	19.50	17.92	17.22	16.82	16.57
82	351.16860962	16.48097610	0.056	4	19.08	19.39	18.77	18.76	18.49	18.43	18.27	18.16	17.88	17.88	17.93	17.67	17.71	17.54	17.48	19.97	18.69	18.12	17.81	17.60
83	351.17163086	16.57984734	0.048	3	21.16	20.21	20.15	19.50	19.25	19.19	18.87	18.84	18.74	18.41	18.43	18.32	18.20	18.11	18.37	20.77	19.48	18.74	18.41	18.16
84	351.21090698	17.24355888	0.060	2	18.82	20.16	19.54	19.82	19.45	19.15	18.99	19.05	18.80	18.59	18.87	18.61	18.81	18.13	18.34	20.96	19.72	18.91	18.79	18.52
85	351.21206665	16.90178680	0.048	1	21.39	19.59	19.38	19.17	18.73	18.62	18.33	18.22	18.03	17.91	17.89	17.79	17.67	17.55	17.29	20.60	19.01	18.05	17.89	17.62
86	351.21966553	16.53191757	0.059	3	19.22	20.53	19.63	19.52	19.03	19.04	19.05	18.67	18.57	18.56	18.40	18.33	18.17	18.28	18.47	24.55	19.46	18.71	18.36	18.12
87	351.22222900	16.40045166	0.017	1	19.30	99.00	19.30	19.94	19.47	19.41	19.31	19.02	18.90	18.56	18.72	18.73	18.60	18.16	18.12	22.09	19.75	19.01	18.69	18.38
88	351.24563599	16.71162224	0.047	3	20.25	19.46	18.89	18.53	18.23	18.14	17.91	17.86	17.61	17.62	17.55	17.47	17.40	17.09	17.14	19.66	18.42	17.82	17.50	17.35
89	351.24801636	17.16534615	0.024	1	23.67	20.18	19.45	19.96	19.62	19.56	19.20	19.13	18.91	18.95	18.70	18.55	18.52	18.26	17.96	21.47	19.93	19.07	18.62	18.38
90	351.26184082	16.57231903	0.023	3	18.84	20.03	20.31	20.80	20.38	20.48	19.75	19.87	19.41	19.58	19.46	19.47	18.72	19.29	99.00	21.78	20.48	19.83	19.44	19.17
91	351.26245117	16.52570343	0.024	1	99.00	99.00	21.90	21.17	20.25	20.81	20.70	19.87	19.49	20.36	19.56	19.69	19.63	99.00	19.79	21.82	20.60	19.96	19.81	19.55
92	351.27828979	16.76721191	0.044	1	19.06	18.34	17.96	17.76	17.63	17.57	17.44	17.36	17.19	17.24	17.24	17.11	17.04	16.98	17.24	19.02	17.72	17.33	17.13	17.03
93	351.28054810	16.81988525	0.029	1	19.76	21.59	19.68	19.32	19.33	19.17	18.97	19.06	18.78	19.34	18.74	18.81	18.52	19.08	19.11	20.63	19.61	19.02	18.82	18.59
94	351.30871582	16.44901848	0.024	2	18.91	19.99	19.60	19.39	19.18	19.07	18.98	18.66	18.48	18.47	18.37	18.25	18.15	17.96	18.00	19.73	19.32	18.69	18.27	18.02
95	351.31192017	16.55031013	0.017	1	19.12	20.74	19.24	18.62	18.41	18.37	17.88	17.83	17.64	17.57	17.59	17.47	17.42	17.29	17.33	20.57	18.61	17.81	17.50	17.33
96	351.36566162	17.25617027	0.048	7	99.00	20.54	21.00	20.06	19.55	19.86	19.31	19.08	19.26	19.51	19.51	19.36	18.81	19.88	19.17	20.47	19.86	19.60	19.51	19.08
97	351.40484619	17.24501801	0.037	2	20.47	20.04	19.57	19.46	19.07	19.01	18.73	18.61	18.37	18.26	18.23	17.94	17.97	18.00	18.11	21.97	19.22	18.56	18.25	18.03
98	351.41052246	16.57383156	0.048	3	20.84	20.53	20.54	19.65	19.35	19.23	99.00	18.92	18.79	18.55	18.84	99.00	18.38	18.14	18.30	20.70	19.60	18.88	18.54	18.24
99	351.41250610	17.13726997	0.045	3	20.05	19.68	19.11	19.24	18.84	18.54	18.43	18.31	18.14	18.18	17.83	17.90	17.80	17.93	17.88	26.46	19.04	18.33	17.97	17.69
100	351.42208862	16.75362396	0.029	1	19.70	20.91	20.45	19.74	19.97	19.86	19.42	19.17	19.08	19.25	18.85	99.00	18.47	18.67	19.07	21.26	20.19	19.20	18.86	18.47
101	351.42596436	16.77386093	0.039	4	19.45	19.22	20.35	19.36	19.23	19.17	18.87	19.01	18.88	18.52	18.62	99.00	18.30	18.49	18.30	20.22	19.36	18.88	18.56	18.54
102	351.42956543	16.78918457	0.046	3	19.33	23.81	20.52	20.13	19.69	19.60	19.31	19.47	19.41	19.18	19.42	99.00	18.68	18.80	19.43	21.38	20.04	19.38	18.97	18.86
103	351.43093872	16.47374535	0.048	3	19.44	23.05	20.24	19.95	19.51	19.50	19.02	19.08	18.80	18.71	18.94	99.00	18.46	18.86	18.50	21.30	19.84	19.16	18.86	18.53
104	351.45364380	16.79960823	0.018	2	99.00	99.00	19.24	19.30	19.18	19.10	18.81	18.77	18.66	18.29	18.40	99.00	18.18	17.97	17.96	20.85	19.39	18.67	18.35	18.08
105	351.45440674	16.41203117	0.029	7	19.82	19.38	19.05	19.26	19.08	18.99	18.90	19.03	18.79	18.89	18.90	99.00	18.67	18.62	18.37	21.07	19.22	18.97	18.79	18.68
106	351.46267700	16.88102722	0.058	3	99.00	20.35	20.28	19.93	19.58	19.59	19.24	19.39	19.26	19.57	19.22	99.00	18.70	19.15	19.89	23.66	19.82	19.35	19.09	19.06

Table 4: Results of κ-test for member galaxies in samples I and II

Neighbor size n	Sample I $P(\kappa_n > \kappa_n^{obs})$	Sample II $P(\kappa_n > \kappa_n^{obs})$
6.........	84.8%	17.8%
7.........	85.9%	21.4%
8.........	81.9%	13.8%
9.........	87.8%	14.5%
10.......	85.2%	21.7%
11.......	85.9%	31.2%
12.......	79.9%	49.2%